Atmos. Meas. Tech. Discuss., 5, 6763–6812, 2012
www.atmos-meas-tech-discuss.net/5/6763/2012/
doi:10.5194/amtd-5-6763-2012


Atmospheric Measurement Techniques Discussions



# Retrieval and validation of $O_3$ measurements from ground-based FTIR spectrometer at equatorial station: Addis Ababa, Ethiopia

**S. Takele Kenea[1], G. Mengistu Tsidu[1], T. Blumenstock[2], F. Hase[2], T. von Clarmann[2], and G. P. Stiller[2]**

[1]Department of Physics, Addis Ababa University, P.O. Box 1176, Addis Ababa, Ethiopia
[2]Institute for Meteorology and Climate Research (IMK-ASF), Karlsruhe Institute of Technology (KIT), Karlsruhe, Germany

Received: 27 July 2012 – Accepted: 22 August 2012 – Published: 18 September 2012

Correspondence to: S. Takele Kenea (samueltake@yahoo.ca)

Published by Copernicus Publications on behalf of the European Geosciences Union.







## Abstract

Since May 2009 high-resolution Fourier transform infrared (FTIR) solar absorption spectra are recorded at Addis Ababa (9.01° N latitude, 38.76° E longitude, 2443 m altitude a.s.l.), Ethiopia. The vertical profiles and total column amounts of ozone ($O_3$) are deduced from the spectra by using the retrieval code PROFFIT (V9.5) and regularly determined instrumental line shape (ILS). A detailed error analysis of the $O_3$ retrieval is performed. Averaging kernels analysis of the target gas shows that the major contribution to the retrieved information always comes from the measurement. We obtained 2.1 degrees of freedom on average for signals in the retrieval of $O_3$ from the observed FTIR spectra. We have compared the FTIR retrieval of ozone Volume Mixing Ratio (VMR) profiles and column amounts with the coincident satellite observations of Microwave Limb Sounding (MLS), Michelson Interferometer for Passive Atmospheric Sounding (MIPAS) and Tropospheric Emission Spectrometer (TES), Ozone Monitoring Instrument (OMI), Atmospheric Infrared Sounding (AIRS) and Global Ozone Monitoring Experiment (GOME-2) instrument. The mean relative differences are generally found below +15 % in the altitude range of 27 to 36 km for comparison of VMR profiles made between MLS and MIPAS, whereas comparison with TES has shown below 9.4 % relative difference. Furthermore, the mean relative difference is positive above 31 km, suggesting positive bias in the FTIR measurement of $O_3$ VMR with respect to MLS, MIPAS and TES. The overall comparisons of column amounts of satellite measurements with the ground-based FTIR instruments show better agreement exhibiting mean relative differences of ground-based FTIR with respect to MLS and GOME-2 within +0.4 % to +4.0 % and corresponding standard deviations of 2.2 to 4.3 % whereas, in the case of OMI, TES, AIRS, the mean relative differences are from −0.38 to −6.8 %. Thus, the retrieved $O_3$ VMR and column amounts from a tropical site, Addis Ababa, is found to exhibit very good agreement with all coincident satellite observations over the 2-yr period.





AMTD
5, 6763–6812, 2012



## 1 Introduction

The composition of the tropical atmosphere and its change is of significant importance for global climate. For several decades, rapid population growth and industrial development, along with deforestation, are increasingly changing the environment in the tropical countries. The effect of these changes on atmospheric composition and climate are quite uncertain, as the governing physical and chemical processes of the tropical atmosphere are only poorly understood. Emissions within the tropics, e.g. from biomass burning or plants, contribute substantially to the global budgets of many important trace gases (IPPC, 2007). Biomass burning is not restricted to the tropics, but most burning occurs in the tropics. The tropics are also the location of two important exchange processes, the interhemispheric exchange and the entry of tropospheric air into the stratosphere.

Ozone is a very important molecule in the middle atmosphere because it absorbs solar ultraviolet (UV) radiation and contributes to the radiative balance of the stratosphere. Thus, the ozone layer protects life on Earth from the harmful and damaging UV solar radiation. Ozone in the lower atmosphere, or troposphere, is also an important greenhouse gas. Tropospheric ozone is formed under high ultraviolet flux conditions from natural and anthropogenic emissions of nitrogen oxides ($NO_x$), volatile organic compounds (VOCs), methane and carbon monoxide Seinfeld and Pandis (2006). Understanding changes occurring in the distribution of ozone in the atmosphere is, therefore, important for studying ozone recovery, climate change and the coupling between these processes WMO (2007).

The tropical NDACC stations at which FTIR measurements are performed are Mauna Loa (19.54° N, 155.6° W), Paramaribo (5.8° N, 55.2° W) and Tarawa (1° N, 173° E). Our measurement site, Addis Ababa (9.01° N latitude, 38.76° E longitude, 2443 m altitude a.s.l.), is also located in the tropics. It is the first high resolution FTIR spectrometer on the African continent. FTIR at Addis Ababa site is planned to be part of NDACC network that has been monitoring long term atmospheric composition changes. In this





AMTD
5, 6763–6812, 2012



study, intercomparison of vertical profiles and column amounts retrieved solar spectra observed by Fourier Transform Spectrometer and that from satellite measurements in different observing modes. The observed differences between observations from ground-based FTIR and satellites are investigated based on a full error characterization and analysis.

The paper is structured as follows: Sect. 2 introduces the measurement site and the FTIR spectrometer. Section 3 provides discussion of spectral analysis. Section 4 details the methodology used for the analysis, and is followed by the detailed intercomparison of the satellite measurements in Sect. 5. Finally, conclusions are given in Sect. 6.

## 2 Measurement site and instrumentation

### 2.1 Measurement site

Addis Ababa is located at 9.01° N latitude, 38.76° E longitude, 2443 m altitude a.s.l., which is in the the equatorial region. It is relatively dry due to its topography, making it robust for monitoring trace species in the tropics as interference of tropospheric water vapor absorption lines is of minor relevance. Moreover, The typical tropopause height for tropical regions is between 16 to 18 km, and the corresponding temperature is about 200 K. The tropical tropopause region is the transition layer between the dynamical control of the vertical mass flux by tropospheric convection, and by the stratospheric Brewer-Dobson circulation (Holton, 2004; Jacobson, 2000). Thus, the site is highly affected by tropical dynamics allowing us to understand processes that modulates tropical dynamics from the observed variation in the measurement of atmospheric trace gases.

### 2.2 The FTIR spectrometer and retrieval

BRUKER interferomenter based on IFS-120 but upgraded with the new electronics of IFS-125M20. Our FTIR interferometer is equipped with mercury-cadmium-telluride





AMTD
5, 6763–6812, 2012



(Hg-Cd-Te) and indiumantimonide (InSb) detectors, which allow coverage of the 600–1500 and 1500–4400 $cm^{-1}$ spectral intervals, respectively. Recently, the new laser source with power supply has been mounted on this interferometer in order to improve the laser signal that reaches to the detector to attain quite stable movement of the optics. Typically, spectral resolution of 0.009 $cm^{-1}$ is applied. FTIR spectrometer makes direct solar absorption observations throughout the day, under clear sky conditions. The spectra are typically constructed by co-adding up to 10 scans recorded in about 8 min. A very large number of species of atmospheric relevance can be detected owing to its wide spectral coverage. In this paper, VMR profiles and column amounts of $O_3$ are derived from measured spectra using version 9.5 of the retrieval code PROFFIT.

PROFFIT was developed to analyze solar absorption spectra measured with high-resolution ground-based FTIR spectrometer; and it has been compared to other retrieval codes Hase et al. (2004). Daily pressure and temperature vertical profiles used in the retrievals are taken from the automailer system of Goddard Space Flight Center. The climatological profiles are based on data from the National Center for Environment Prediction (NCEP). Spectroscopic data are taken from the High Resolution Transmission data (HITRAN) 2004 database Rothman et al. (2005). PROFFIT includes various retrieval options such as scaling of a priori profiles, the Tikhonov-Phillips method (Phillips, 1962; Tikhonov, 1963), or the optimal estimation method (Rodgers, 1976).

The retrieved state vector contains the retrieved logarithm of volume mixing ratios of the target gas defined in discrete levels in the atmosphere and retrieved interfering species column amounts, and fitted values for some model parameters. These include the baseline slope and instrumental line shape parameters. The retrieval of $O_3$ profiles is performed on a logarithmic scale because $O_3$ concentration around the tropopause are highly variable. Under these conditions a logarithmic scale inversion is superior to a linear inversion (Hase et al., 2004; Schneider et al., 2006a).

As discussed in Rodgers (2000), the optimal estimation method allows the characterization of the retrievals, i.e. the vertical resolution of the retrieval, its sensitivity to the a priori information and degree of freedoms for signal (DOFs). The retrieved state





AMTD
5, 6763–6812, 2012



vector $\hat{\boldsymbol{x}}$ is related to the a priori and the true state vectors $\boldsymbol{x}_a$ and $\boldsymbol{x}$, respectively, by the equation

$$\hat{\boldsymbol{x}} = \boldsymbol{x}_a + \hat{\mathbf{A}}(\boldsymbol{x} - \boldsymbol{x}_a) + \text{error terms} \quad (1)$$

where $\hat{\mathbf{A}}$ is averaging kernel matrix. The actual averaging kernels matrix depends on several parameters including the solar zenith angle, the spectral resolution and signal to noise ratio, the choice of retrieval spectral microwindows, and the a priori covariance matrix $\mathbf{S}_a$. The elements of the averaging kernel for a given altitude give the sensitivity of the retrieved profile at that altitude to the real profile at each altitude, and its full width at half maximum is a measure of the vertical resolution of the retrieval at that altitude Vigouroux et al. (2007). Error estimation analysis based on the analytical method suggested by Rodgers (Rodgers, 2000):

$$\hat{\boldsymbol{x}} - \boldsymbol{x} = (\hat{\mathbf{A}} - \mathbf{I})(\boldsymbol{x} - \boldsymbol{x}_a) + \hat{\mathbf{G}}\hat{\mathbf{K}}_p(\boldsymbol{p} - \hat{\boldsymbol{p}}) + \hat{\mathbf{G}}\epsilon \quad (2)$$

where $\hat{\boldsymbol{p}}$, $\boldsymbol{p}$ are the estimated and real model parameters, respectively, $\hat{\mathbf{G}}$ is the gain matrix, $\hat{\mathbf{K}}_p$ is the model parameter sensitivity matrix and $\epsilon$ represents noise. The first term in Eq. (2) represents the smoothing error that is the main source of error for vertical concentration profiles. The second term stands for the estimated error due to uncertainties in input parameters, such as instrumental parameters or spectroscopic data, the $\boldsymbol{p} - \hat{\boldsymbol{p}}$ is only valid for fully correlated perturbations of $\boldsymbol{p}$ (assuming that $\boldsymbol{p}$ is a vector). In addition, the third term represents the error due to the measurements noise.

The full width at half maximum of absorbtion lines of stratospheric gases and of ILS have similar magnitudes. Therefore, instrumental line shape (ILS) needed for accurate retrieval was derived from regular cell measurements using the LINEFIT software Hase et al. (1999). Using the globar as a source of IR radiation, up to 100 scans are coadded to get spectra of both with and without the presence of HBr cell placed in the parallel beam of a radiation source. The LINEFIT software was used to compute ILS





AMTD
5, 6763–6812, 2012



by comparing the measured line shape with the theoretical one. We obtained modulation efficiency and phase error during the measurement period May, 2009 to February 2011 as in Fig. 4. Figure 4 illustrates that the modulation efficiency remains nearly constant with minor fluctuation over a range of 98–100 %. The phase error is also confined to ±0.02 rad. Therefore, there was an excellent instrumental alignment for a period of more than 2 yr considered in this study.

## 3 Information content and error analysis

This section discusses information on the retrieval of vertical distribution and column amount of $O_3$ from ground-based high resolution FTIR spectra because it is related to the pressure broadening of the absorption lines. While the line centers provide information about the higher altitudes of the distribution, the wings of a line provide information about the lower altitudes. Therefore the information content of the retrieval will strongly depend on the choice of the absorption lines. The other important requirement that has been taken into consideration to perform this task successfully is a good knowledge of pressure and temperature profiles. Sensitivity of retrieval as function of altitude and over error budget have been analyzed thoroughly to ensure information coming from the measurement overweighs that from the a priori in as much as possible in a trade off procedure between getting smoothed profile and enhancing information from measurement. Spectral microwindows found to be best in this sense for $O_3$ retrievals are those near 3041, 3045 and 3051 $cm^{-1}$ for the InSb measurements having high sensitivity in the stratosphere and almost no sensitivity in the troposphere. The microwindows near 1000 $cm^{-1}$ is best suited for the retrieval of ozone since it has highest sensitivity to both the stratosphere and troposphere which has been reported in different papers (Barret et al., 2002, 2003; Lindenmaier et al., 2010) for the MCT measurement, however, in our case, we have far more number of InSb measurements than MCT measurements. In this analysis, we considered six microwindows in the spectral region between 3039.37 to 3051.90 $cm^{-1}$.





AMTD
5, 6763–6812, 2012



The major absorption lines of interfering gases are $H_2O$ and $CH_4$. There are also minor interferences from $CH_3D$, $CH_3Cl$, $C_2H_4$ and solar lines. Figure 1 shows example of measured spectra (black line), the corresponding simulated spectra (red) and the residual spectra in each microwindows for one of the measurements taken on 27 May 2010. The magnitude of residual spectra grows up to a maximum of 1.5 % in the positive and in the negative part of the plot.

Figure 2 (left panel) shows averaging kernel matrix while its rows shown in different colors (right panel) depicts the same thing but response in two different altitude ranges are clearly indicated by different color coding. For ideal retrieval for which the ozone profile is purely determined by measurement, the averaging kernel will be unit matrix. The full width at half maximum of the rows of the averaging kernel gives the vertical resolution, which is in the order of 9–15 km for the retrieved $O_3$ in this study. The sensitivity of the spectra to perturbation in VMR at each height is shown by well defined and sharp rows of the averaging kernel. This means that the retrievals of $O_3$ are mainly sensitive in the altitude range 16 to 40 km as indicated in Fig. 2. Furthermore, the trace of the averaging kernel matrix, the so called degree of freedom for signals, provides another useful measure retrieval quality of target species. The independent pieces of information retrieved from the observed spectra in the $O_3$ spectral microwindows under the given retrieval strategy contain about 2.1 degree of freedom for signals (dofs). This provides 2 independent layers, which approximately covers the altitude range of 2.5 to 26 km and 26 to 40 km as marked by basically two dominant peaks of rows of averaging kernel in Fig. 2 (right panel). The value of dofs obtained in this study is relatively small as compared to the values reported in the literatures (e.g. Lindenmaier et al., 2010; Schneider et al., 2005a). Different amount of degree of freedom for signals can be obtained due to application of different microwindows with different spectral resolution and the choice a priori covariance matrix. Wunch et al. (2007) reported 2.1–2.4 dofs for ozone retrieval by applying microwindows near 2775 and 3040 $cm^{-1}$ with different spectral resolution during instruments intercomparison campaign at University of Toronto, which confirms our result. The spectral resolution of our instrument that we





AMTD
5, 6763–6812, 2012



applied at this tropical site could give this degree of freedom for signals because the tropopause level in tropical region is high.

As discussed in Sect. 2, the contribution of different sources of errors that contribute to the quality of measurement of the target gas is displayed in Fig. 3. Figure 3 shows the statistical error (left panel) and systematic error (right panel) profiles for a typical $O_3$ retrieval. The major sources of errors quantified in this study include temperature, noise, instrumental line shape, solar lines, line of sight, baseline, and spectroscopy. One can note from Fig. 3 that the main systematic error source is the uncertainty of spectroscopic parameters, whereas the major statistical error source is noise. The contribution of error from uncertainty in solar lines and line of sight to $O_3$ profile retrieval is the lowest. The maximum estimated systematic and statistical error budget reach up to 0.6 ppmv around 31 km and 0.2 ppmv at 35 km respectively. The main systematic error sources for partial columns for the $O_3$ retrieval from ground-based FTIR is $O_3$ line intensities and air broadening coefficients (Barret et al., 2002, 2003) which could partly explain the observed biases. Whenever averages are calculated on the basis of log retrievals, this leads to biases (Funke and von Clarmann, 2012). There is an impact of averages on the basis of log retrievals in the result of $O_3$ in this study. By adding up systematic and statistical error sources for a given altitude and then integrating it along the error patterns (Rodgers, 2000), we obtained the total systematic and random error on FTIR $O_3$ total columns to 2.1 % and 0.8 %, respectively. The total systematic error on the total columns is in good agreement with those found in (Viatte et al., 2011 and reference therein). But the total random error for the total column estimated in this study is 0.3 % higher than those reported by Viatte et al. (2011), this difference may come from the considered retrieval parameters during retrieval.





AMTD
5, 6763–6812, 2012



## 4 Satellite measurements

### 4.1 Microwave Limb Sounder (MLS)

The Earth Observing System (EOS) Microwave Limb Sounder (MLS) is one of four instruments on the NASA EOS Aura satellite (Schoeberl et al., 2006), launched on 15 July 2004 into a near polar sun-synchronous orbit at 705 km altitude, with ascending equatorial crossing time of 13:45 (local time). The Aura-MLS instrument, calibration and performance for the different channels are described by Jarnot et al. (2006). It scans the Earths limb providing 240 scans per orbit, spaced ~ 165 km along the orbit track, and 3500 vertical profiles per day for 17 primary atmospheric parameters: pressure, temperature and cloud ice water content, as well as 14 trace constituents such as $O_3$, $H_2O$ and CO, with near pole-to-pole global latitudinal coverage from 82° S to 82° N. MLS measures thermal emission lines from limb, using seven radiometers to provide coverage of five spectral regions between 118 GHz and 2.5 THz, during both day and night. The retrieval scheme is based on the optimal estimation method (Rodgers, 2000). This retrieval approach is detailed by (Livesey et al., 2006). We used the recommended parameters for screening the Aura-MLS data for the target trace gas of $O_3$.

In this work, we have used the version 2.2 of MLS $O_3$ dataset for validation of FTIR result. The MLS version 2.2 $O_3$ profiles is the standard ozone product retrieved from radiance measurements near 240 GHz. It has been extensively characterized and validated (Froidevaux et al., 2008; Jiang et al., 2007; Livesey et al., 2008). The vertical resolution is estimated to be ~ 3 km in the upper troposphere and stratosphere, but degrades to 4 to 6 km in the upper mesosphere and the horizontal resolution is about 200–300 (along the track). The precision is estimated to be 10–30 % (0.3 ppmv) at 0.2–1 hPa, 2–5 % (0.1–0.2 ppmv) at 2–46 hPa, and 0.04 ppmv (2–100 % since the ozone values vary a lot) at 68–215 hPa. More details regarding the MLS experiment and $O_3$ data screening are provided in the above references in detail and at http://mls.jpl.nasa.gov/data/datadocs.php.





AMTD
5, 6763–6812, 2012



### 4.2 Michelson Interferometer for Passive Atmospheric Sounding (MIPAS)

The MIPAS instrument is a high-resolution atmospheric limb sounder aboard ESAs ENVISAT launched in March 2002 and operating in a sun-synchroneous orbit. It aims at global and simultaneous measurements of the chemical composition of the middle atmosphere and upper troposphere. By means of sounding the Earths limb in the mid infrared it gathers emission spectra during night and day time conditions. Nearly global coverage is achieved within three days. For this purpose, it acquires spectra in five frequency bands over the range 685–2410 $cm^{-1}$ (14.6–4.15 µm). The pointing system allows MIPAS to observe atmospheric parameters in a maximum altitude range of 5–160 km with a vertical spacing of 1–8 km depending on the altitude and on the measurement mode (Fischer et al., 2008). Operational measurements at full spectral resolution (0.025 $cm^{-1}$) were conducted from July 2002 to March 2004. However, anomalies affecting the interferometer slide mechanism led to the suspension of operations on 26 March 2004. Observations were resumed in January 2005 with a new operation mode, on a finer vertical grid and with reduced spectral resolution (0.0625 $cm^{-1}$). The vertical resolution of MIPAS ozone is increasing from 3.5 km at 10 km altitude to about 5 km at 42 km, and around 8 km at 60 km altitude.

In this study, we have used the reduced spectral resolution (Institute for Meteorology and Climate Research) IMK/IAA MIPAS ozone data product V5R_O3_220 (von Clarmann et al., 2009) for validation purpose. The first validation of reduced resolution IMK/IAA ozone data was reported by Stiller et al. (2012).

### 4.3 Tropospheric Emission Spectrometer (TES)

The Tropospheric Emission Spectrometer (TES) launched into sun-synchronous orbit on aboard Aura, the third of NASAs Earth Observing System (EOS) spacecraft, on 15 July 2004. TES is an infrared high spectral resolution (0.1 $cm^{-1}$ apodized in nadir) Fourier Transform Spectrometer (FTS) with both limb and nadir sounding capabilities (Beer et al., 2001). TES will record the Earths spectral radiance from discrete locations





AMTD
5, 6763–6812, 2012



along the orbit track in the wave number range 650 to 2250 $cm^{-1}$ (15.4 to 4.4 mm). The spectral radiances measured by TES are used to retrieve the atmospheric profiles through a nonlinear optimization algorithm that minimizes the difference between observed radiances and those calculated with a Radiative Transfer Model (RTM), subject to the condition that the solution is consistent with an a priori description of the atmosphere (Rodgers, 2000; Bowman et al., 2002, 2006). The standard products that will be retrieved from these spectra are vertical concentration profiles of ozone, water vapor, carbon monoxide, methane, nitric oxide, and nitric acid. The global survey mode includes both daytime and nighttime ozone measurements. For cloud free conditions, the vertical resolution of TES ozone profile retrievals is typically 6 km in the tropics (Clough et al., 2002; Worden et al., 2004). TES level 3 data with grid spacing 2° latitude and 4° longitude is used for validation purpose in this work. TES ozone data have been evaluated by comparison to ozonesondes (e.g. Nassar et al., 2008; Worden et al., 2007), aircraft data (e.g. Richards et al., 2008), and ozone measured by other satellite instruments (e.g. Zhang et al., 2010).

### 4.4 Ozone Monitoring Instrument (OMI)

Ozone Monitoring Instrument, is one of the four instruments on EOS-Aura. OMI is a Dutch-Finnish built nadir-viewing pushbroom UV/visible instrument. It measures backscattered radiances in three channels covering the 264–504 nm wavelength range (UV-1: 264–311 nm, UV-2: 307–383 nm, visible: 349–504 nm) at spectral resolutions of 0.42–0.63 nm Levelt et al. (2006). OMI has a wide field of view (115°) with a cross track swath of 2600 km. Measurements across the track are binned to 60 positions for UV-2 and visible channels and 30 positions for the UV-1 channel (due to weaker signals). This results in daily global coverage with a spatial resolution of 13 km × 24 km (along × across track) at the nadir position for UV-2 and visible channels, and 13 km × 48 km for the UV-1 channel. It measures OC, ozone profile, and the total abundances of other





AMTD
5, 6763–6812, 2012



trace gases (e.g. $NO_2$, $SO_2$, HCHO, BrO, CHOCHO, OClO), as well as UV absorbing aerosols and clouds (Liu et al., 2010).

Profiles of partial ozone column densities in 24 layers from the surface to 60 km are retrieved from OMI radiances in the spectral region 270–330 nm using the optimal estimation technique. Retrievals contain 6–7 degrees of freedom for signal (Rodgers, 2000), with vertical resolution generally varies from 3965 km. In this study, we have used OMI level 3d ozone total column amounts with grid spacing 1° longitude and 1° latitude for comparisons. Overall the quality of total ozone data provided in OMTO3 should have a root-mean squared error of 1–2 %, depending on solar zenith angle, aerosol amount, and cloud cover. More details about the instrument and its scientific objectives can be found in the Science Requirements Document for OMI-EOS Levelt et al. (2000). OMI total ozone column measurements has been evaluated by comparison to Brewer and Dobson spectrophotometer ground-based observations Balis et al. (2007).

### 4.5 Atmospheric Infrared Sounding (AIRS)

The Atmospheric Infrared Sounder (AIRS) instrument is one of several instruments onboard the Earth Observing System (EOS) Aqua spacecraft launched 4 May 2002. It is comprised of a space-based hyperspectral infrared instrument (AIRS) and two multichannel microwave instruments, the Advanced Microwave Sounding Unit (AMSU-A) and the Humidity Sounder for Brazil (HSB). The HSB instrument ceased operation on 5 February 2003. AIRS is a high spectral resolution spectrometer on board Aqua satellite with 2378 bands in the thermal infrared (3.7–15.4 µm) and 4 bands in the visible (0.4–1.0 µm). The AIRS instrument operates to scan the Earth's atmosphere in nadir viewing. AIRS daily level 3 version 5 $O_3$ standard products are used for validation and its spatial resolution is 1° latitude and 1° longitude. Each level 3 daily product contains information for a temporal period of 24 h for either the descending or ascending orbit (rather than midnight-to-midnight) where ascending or descending refers to the direction of movement of the sub-satellite point in the satellite track at the equatorial





AMTD
5, 6763–6812, 2012



crossing. The ascending direction of movement is from Southern Hemisphere to Northern Hemisphere, with an equatorial crossing time of 01:30 p.m. local time; the descending direction of movement is from Northern Hemisphere to Southern Hemisphere, with an equatorial crossing time of 01:30 a.m. local time. AIRS/AMSU/HSB will observe and characterize the entire atmospheric column from the surface to the top of the atmosphere in terms of surface emissivity and temperature, atmospheric temperature and humidity profiles, cloud amount and height, and the spectral outgoing infrared radiation. Paper regarding an overview of the AIRS Radiative Transfer Model has been published by Strow et al. (2003). Further details about the overview of AIRS instruments can been found in Young-In Won (2008) and at http://disc.gsfc.nasa.gov.

### 4.6 Global Ozone Monitoring Experiment (GOME-2)

The Global Ozone Monitoring Experiment (GOME-2) aboard MetOp-A is a scanning spectrometer that captures light reflected from the Earths surface and backscattered by the atmosphere. The spectrometer splits the light into its spectral components covering the UV/VIS region from 240 nm to 790 nm at a resolution of 0.2 nm to 0.4 nm. In particular, the nominal spectral resolution of GOME-2 in the spectral range 325–335 nm used for $O_3$ fitting is slightly below 0.24 nm. The measured spectra are mainly used to derive ozone total columns and vertical profiles, as well as concentrations of nitrogen dioxide, bromine monoxide, water vapor, sulfur dioxide and other trace gases, and also cloud properties and aerosols. The GOME-2/MetOp field of view of each step may be varied in size from 5 km × 40 km to 80 km × 40 km. The mode with the largest footprint (twenty four steps with a total coverage of 1920 km × 40 km) provides daily near global coverage at the equator.

The algorithm for $O_3$ retrieval, GOME Data Processor (GPD), version 4.2 has been used based on two methods: the DOAS (Differential Optical Absorption Spectroscopy) method Platt (1994), and the iterative AMF/VCD (Air Mass Factor/Vertical Column Density) computation Van Roozendael et al. (2006). Error analysis indicates an accuracy and precision of $O_3$ total columns of 3.6–4.3 % and 2.4–3.3 %, respectively





AMTD
5, 6763–6812, 2012



when the solar zenith angle is below 80° Van Roozendael et al. (2004). Total ozone columns derived from this algorithm have been validated using ground-based networks (Balis et al., 2007b, 2008). Further details of the document can be obtained from: http://wdc.dlr.de/sensors/gome2. In this paper, we have used $O_3$ columns from GOME-2 level 3 data.

## 5 Validation of FTIR $O_3$ VMR profiles and column amount against MLS, MIPAS, TES, OMI, AIRS and GOME-2 observations

### 5.1 Validation methodology

The closest satellite measurements (on the same day as the ground-based FTIR) within ±2 degrees of latitude and ±10 degrees of longitude are selected. The more stringent latitudinal criterion has proven to be a good choice for all comparisons, since latitudinal variations are in general more pronounced than longitudinal ones. Based on the fact that these criteria yielded 76, 14, 13, 70, 70 and 46 days of coincident measurements between FTIR and MLS, MIPAS, TES, OMI, AIRS and GOME-2, for respectively. All the satellite data (MLS, MIPAS, TES, OMI, AIRS and GOME-2) used in the following comparisons have considerably better vertical resolution than ground-based FTIR profiles due to observation geometry, spectral windows and measurement techniques in a netshell. The vertical resolution of satellite measurements of profiles are therefore degraded to facilitate a comparison between the two sets of profiles. Therefore, the satellite measurement profiles are smoothed using the averaging kernels calculated during the ground-based FTIR retrieval process as proposed by Rodgers and Connor (2003). Since then the method has been applied by many authors for intercomparison of satellite observations of different resolutions and observations from other plateforms such as aircraft, ballon and from ground (e.g. Hoogen et al., 1999; Lucke et al., 1999; Schneider et al., 2002; Mengistu Tsidu, 2005). The equation relating FTIR and satellites can be given by





AMTD
5, 6763–6812, 2012



$$\hat{\boldsymbol{x}}_{\mathrm{s}} = \boldsymbol{x}_{\mathrm{a}} + \hat{\mathbf{A}}_{\mathrm{FTIR}}(\boldsymbol{x}_{\mathrm{Sat}} - \boldsymbol{x}_{\mathrm{a}}) \quad (3)$$

where $\boldsymbol{x}_{\mathrm{Sat}}$ is the original satellite measurement profile, $\boldsymbol{x}_{\mathrm{s}}$ is the smoothed profile, and $\boldsymbol{x}_{\mathrm{a}}$ and $\hat{\mathbf{A}}_{\mathrm{FTIR}}$ are the a priori profile and the averaging kernel matrix of the ground-based FTIR instrument, respectively. To calculate the profile of the mean absolute difference, the differences are calculated for each pair of profiles at each altitude, and then averaged at altitude $z$ as

$$\Delta_{\mathrm{abs}}(z) = \frac{1}{N(z)} \sum_{i=1}^{N(z)} [\mathrm{FTIR}_i(z) - \mathrm{Sat}_i(z)] \quad (4)$$

where $N(z)$ is the number of coincidences at $z$, $\mathrm{FTIR}_i(z)$ is the FTIR VMR at $z$ and the corresponding $\mathrm{Sat}_i(z)$ VMR for the validation instrument. Note that the term absolute, as used in this work, refers to differences between the compared values, in VMR as opposed to percentage or relative differences, in other words: absolute differences can well be negative. To calculate the profile of the mean relative difference, as a percentage, we used

$$\Delta_{\mathrm{rel}}(z) = 100(\%) \times \frac{1}{N(z)} \sum_{i=1}^{N(z)} \frac{[\mathrm{FTIR}_i(z) - \mathrm{Sat}_i(z)]}{[\mathrm{FTIR}_i(z) + \mathrm{Sat}_i(z)]/2} \quad (5)$$

In some cases, there seems to be a discrepancy between the apparent differences given by the sign of the mean absolute and mean relative differences. Having in mind that the mean relative differences are not calculated from the mean VMR profiles but from each pair of coincident profiles (Eq. 4). Thus, the mean relative differences can become negative, even though the mean absolute differences are positive. A comparison of the total column amounts between FTIR and its correlative measurements has been done by employing the FTIR averaging kernels for smoothing. The relative differences of the total column amounts between FTIR and its correlative measurement from MLS, TES, OMI, AIRS and GOME-2 instrument for coinciding dates is defined as





AMTD
5, 6763–6812, 2012



$$\text{Rel. diff.}(\%) = \left(\frac{[\text{FTIR}_i(\text{TC}) - \text{Sat}_i(\text{TC})]}{[\text{FTIR}_i(\text{TC}) + \text{Sat}_i(\text{TC})]/2}\right) \times 100 \quad (6)$$

where TC represents total column amount and $\text{Sat}_i(\text{TC})$ refers correlative satellite measurement. Moreover, data are screened to reject either the whole profile or identified low-quality measurements at some altitudes from each instrument according to the recommendations provided by each calibration/processing team.

### 5.2 Comparison of FTIR and MLS

Figure 5 shows example of comparison of $O_3$ profiles between ground-based FTIR and MLS version 2.2 on 27 May 2010. Middle and right panels of Fig. 5 depict the absolute difference between FTIR and smoothed MLS profiles of $O_3$ and its relative (fractional) differences respectively. FTIR measurements are slightly greater than MLS measurements above 31 km altitude. Figure 6 shows the statistical relationship for all 76 coincidences for $O_3$. The left-hand side shows the mean absolute differences (ppmv) and the right-hand side is mean relative differences (%). Error bars represent the standard deviation. The mean relative differences are within −6.7 to +20 % above 16.6 km. In general, it is noted that FTIR measurement has a negative bias in the altitude between 16.6 and 28.5 km, and a positive bias above 28.5 km with respect MLS.

Figure 7 depicts the comparisons of daily time series of $O_3$ stratospheric columns of FTIR and MLS (not smoothed). The upper panel in Fig. 7 shows the results of FTIR measurements and of collocated MLS data while in the lower panel, the relative difference between them is displayed. The time series of the $O_3$ column amounts derived from FTIR, particularly during May 2009 is relatively higher than values at other times. During May 2009, the spectra that were recorded at the solar zenith angle (SZA) of around 15° is used that led to high amount of ozone. As evident from Table 2, a mean relative difference of $(3.9 \pm 4.3)$% reveals that there is significant but small difference between the FTIR and MLS results. In general, FTIR column amounts are about 3.9 %





AMTD
5, 6763–6812, 2012



higher than MLS values which is higher than the total uncertainty of FTIR $O_3$ column amounts of the measurement. The correlation coefficient between FTIR and MLS column amount is also depicted in Fig. 16a. The correlation coefficient of 0.81 suggests strong relationship between the two datasets.

The validation of FTIR measurements of $O_3$ amounts have been done with different instruments such as Brewer spectrometer (Schneider et al., 2005a) with very small differences in contrast to satellite measurements from Improved Limb Atmospheric Spectrometer-II (ILAS-II) (Griesfeller et al., 2006) with the relative differences within 10 to 15 % for vertical VMR profiles. Other validation papers, for example, the mean relative differences between ACE-FTS and ground-based FTIR vary between −14 and +12 %, in the middle troposphere (∼ 6 km) up to the stratopause (∼ 47 km) reported by Senten et al. (2008), which in general supports the results presented here. Some of the differences between the FTIR and MLS could have arisen from local and spatial differences in the measurements, even though there is no large variability in space and time during taking coincident measurement. Tropics are well characterized by strong dynamics so that it could contribute for the variation of ozone amount. As reported by Ture (2011), there is also strong interaction between tropics and midlatitude as well as stratosphere-troposphere exchange during Rossby wave breaking bringing in rich ozone airmass into the tropics. Furthermore, different spectroscopic windows used by FTIR and other instruments used for this validation might have also some contribution to the observed differences.

### 5.3 Comparison of FTIR and MIPAS

The comparison of ozone profiles between FTIR and MIPAS has analyzed in the altitude between 11.7 and 40 km have been analyzed. Figure 8 shows that the comparison of $O_3$ profiles from ground-based FTIR with MIPAS IMK/IAA ozone profiles (version V5R_O3_220) on 26 May 2010. Figure 8 (middle and right panels) depicts the absolute difference between FTIR and smoothed MIPAS profiles of $O_3$ and its relative (fractional) differences respectively. FTIR $O_3$ VMRs are slightly greater than MIPAS measurements





AMTD
5, 6763–6812, 2012



above 35 km. The magnitude of the largest absolute difference is 1.7 ppmv (−20.4 %) around 27.7 km. Figure 9 shows the statistical relationship for 14 coincident measurements. Figure 9 (left panel) shows the mean absolute differences (ppmv) and mean relative differences (left panel in %). The mean relative differences are within ±20 % above 23 km. Comparison shown vary significantly between the lower stratosphere, where dynamics and chemistry interfere, with clear influences of tropospheric dynamics, and the higher stratosphere, where photochemistry dominates. The larger differences observed at the lower part of the comparison can be associated, as already noticed, to the effects of strong atmospheric gradients in the Upper Troposphere Lower Stratosphere (UTLS). It is noted that FTIR measurement has a negative bias below the altitude below 32.4 km and a positive bias above 32.4 km. Furthermore, the discrepancy of the result could be partly explained by known contributions to the systematic error budget of the comparison. As compared to other previous comparison study, for example, Steck et al. (2007) compared MIPAS $O_3$ VMR profiles with ground-based FTIR over different stations and found the mean differences within ±10 % in the middle stratosphere, which is also comparable to the differences found in the comparison of $O_3$ VMR profiles of FTIR with MIPAS in this study.

### 5.4 Comparison of FTIR and TES

Figure 10 shows example of the comparison of $O_3$ profiles derived from ground-based FTIR with profiles from TES at Addis Ababa on 27 May 2010. The comparison result in Fig. 10 reveals that FTIR measurements are slightly greater than TES measurements above 31 km. The largest absolute difference is about 1.0 ppmv and the corresponding relative discrepancy is about 14 % at the altitude of 38.8 km. Figure 11 shows the statistical relationship for 13 coincidences for $O_3$ profiles for the mean absolute differences (ppmv) and mean relative differences (right panel in %). The mean relative differences lie between −4.4 to +9.4 % in the altitude range of 11.7–36.3 km where the mean absolute differences are within −0.2 ppmv to +0.8 ppmv. From the overall comparison results, it can be noted that FTIR measurement has a positive bias in the





AMTD
5, 6763–6812, 2012



altitude below 18.3 km and above 27.7 km and a negative bias between 18.3–27.7 km. TES ozone data have been evaluated by comparison to ozonesondes (e.g. Nassar et al., 2008; Worden et al., 2007). For example, Nassar et al. (2008) reported the bias exceeds 20 % at low altitudes over tropics, which confirms our results presented here. This tropospheric biases agreed with the evaluation of TES ozone using airborne differential absorption LIDAR (Richards et al., 2008).

FTIR $O_3$ total columns are also validated against TES measurement. Figure 12 displays the comparisons of time series of $O_3$ total columns of FTIR and TES. Figure 12 (upper panel) depicts the results of FTIR and of collocated TES column amounts and the lower panel shows relative difference. On 13 occasions, the mean relative difference of FTIR data is $(-2.6 \pm 10.5)$%. This would suggest that it is in good agrement. We did not compute the correlation coefficient because the sample size is small.

### 5.5 Comparison of FTIR and OMI

In this section, the comparison of retrieved $O_3$ total column amounts of FTIR with OMI measurement has been reported. Figure 13 shows the comparisons of time series of $O_3$ total columns of FTIR and OMI over Addis Ababa. Based on the coincidence criteria, 70 coincident days are found. The overall mean relative difference between FTIR and OMI shown in Table 2 is $(-0.4 \pm 6.3)$%. This discrepancy could be explained by the application of UV and IR spectroscopy of ozone during retrieval. The mean relative difference of our result is slightly higher than the mean relative differences of the previous comparisons between FTIR and OMI made by Viatte et al. (2011). The FTIR measures systematically higher $O_3$ total columns than the OMI instrument, which may be due to inconsistencies in the spectroscopic parameters (Viatte et al., 2011 and reference therein). Figure 16b shows a good correlation of 0.77 between FTIR and OMI data for the coincident periods. Moreover, as stated in Sect. 5.2, the temporal variation of the measurement could also contribute for the discrepancy of the comparison over tropical site since tropics is well characterized by strong dynamics.





AMTD
5, 6763–6812, 2012



### 5.6 Comparison of FTIR and AIRS

The comparisons of $O_3$ column amounts between FTIR and AIRS have been discussed in this section. Figure 14 depicts the comparison of $O_3$ total columns of FTIR and AIRS. The upper panel in the plot shows the results of FTIR measurements and of collocated AIRS data. The 70 coincident days are found based on the coincidence criteria given in this Section. The lower panel shows the relative difference between FTIR and AIRS total column. The relative differences between the FTIR and AIRS total column are generally within ±15 %. This suggests that the absolute difference of the column amount is bounded within $\pm 1.3 \times 10^{18}$ mol cm$^{-2}$. In general, the mean relative difference is $(-6.8 \pm 7.6)$% (see Table 2) which suggests a slight underestimation $O_3$ columns by FTIR. To further understand the implication of the biases in the comparison between FTIR and AIRS data, we examined the correlation between the instruments. Figure 16c displays the correlation between FTIR and AIRS column amounts of $O_3$ for the given coincident data as characterized by correlation coefficient of 0.70 and slope of the linear regression of 0.77. The relative difference between FTIR and AIRS is found to be consistent with the literature reported by Dupuy et al. (2009) during the comparison between ACE-FTS and ground-based FTIRs. As stated in the previous sections, tropical dynamics could also partly contribute for the disagreement between FTIR and AIRS comparison of total column amounts.

### 5.7 Comparison of FTIR and GOME-2

The validation of FTIR $O_3$ column amounts against GOME-2 measurements has been done. Figure 15 depicts the comparisons of $O_3$ total columns between FTIR and GOME-2. The upper panel shows the comparison of time series of $O_3$ total column amounts on both instruments. Based on the coincidence criteria, 46 coincident days are found. The lower panel shows the relative difference between FTIR and GOME-2 total column amounts. As can be seen in the plot, the maximum relative differences are observed on few coincident measurements during 2009. In general, the mean relative





AMTD
5, 6763–6812, 2012



differences between FTIR and GOME-2 total columns are 0.5 ± 2.2 %. This indicates that there is better agreement between FTIR and GOME-2 measurements. The most likely explanation for this is a bias in the UV and IR spectroscopy of ozone. The mean relative difference of 1.8 % is agreed with the previous comparison study Viatte et al. (2011). The positive sign of mean relative differences appearing in the comparison suggest that the IR ground-based measurements over-estimate the $O_3$ total column amounts. This trend confirms the systematic difference between IR and UV measurements.

## 6 Conclusions

Ground-based FTIR spectrometer is a very useful technique to derive total column amounts and vertical profiles of many important trace gases in the atmosphere. This measurement site located at Addis Ababa (9.01° N latitude, 38.76° E longitude, 2443 m altitude a.s.l.), is a tropical site which will complement previous two sites. As it provides unique information on the African continent, these measurements are of great importance for a better understanding of global climate and physical and chemical processes of the tropical atmosphere as well as for satellite validations. The instrument characteristics are regularly determined i.e. on average about every one month. The instrument is found to be quite stable from analysis of modulation efficiency and phase errors during the whole measurement period even though there were adjustments made in detector and improving laser signal that controls the movement of the scanner.

The closest satellite measurements (on the same day as the ground-based FTIR) within ±2 degrees of latitude and ±10 degrees of longitude are selected. These criteria yielded 76, 14, 13, 70, 70 and 46 days of coincident measurements between FTIR and MLS, MIPAS, TES, OMI, AIRS and GOME-2, for respectively. All the satellite data (MLS, MIPAS, TES, OMI, AIRS and GOME-2) used in the following comparisons have considerably better vertical resolution than ground-based FTIR profiles. The resolution of ozone profiles from the satellites are degraded to the FTIR resolution after





AMTD
5, 6763–6812, 2012



convolving with FTIR $O_3$ averaging kernel for the validation purpose. The agreement determined from an intercomparison of $O_3$ profiles and column amounts of FTIR and the satellites instruments are found to be very good. For instance, the comparison of FTIR $O_3$ with that of MLS yields the mean relative differences of −6.7 to +18.8 % between 16.6 and 39.1 km. Comparison with MIPAS shows mean relative difference of ±18.4 % above 24.8 km. Similarly, in comparison of FTIR with TES, the mean relative differences/absolute differences lie between −4.4 to +9.4 % (−0.2 ppmv to +0.8 ppmv) in the altitude range of 11.7–36.3 km. Furthermore, the mean relative difference is positive above 31 km, suggesting positive bias in the FTIR measurement of $O_3$ VMR with respect to MLS, MIPAS and TES. In general, a low bias is observed at the region of peak ozone concentration. On the other hand, the larger biases are seen in the UTLS, which is partly explained by the effect of strong atmospheric gradients.

Measurement differences have also been shown by other studies and could be compared with the results of this study. Griesfeller et al. (2006) compared Improved Limb Atmospheric Spectrometer-II (ILAS-II) VMR profiles with FTIR and found differences of 10–15 %, which is comparable to the differences found in the comparison of $O_3$ VMR profiles between FTIR and MLS. Other independent comparison study, for example, Nassar et al. (2008) validated TES ozone profiles against ozonesondes and obtained the bias exceeds 20 % at low altitudes over tropics, which confirms our results presented here.

The overall comparisons of column amounts of satellite measurements with the ground-based FTIR instruments show better agreement with mean relative differences of MLS and GOME-2 within +0.2 % to +4.9 % and corresponding standard deviations of +0.4 % to +4.0 %; whereas, in the case of OMI, TES, AIRS, the mean relative differences are from −0.4 to −6.8 %. Those comparison results have also been compared with previous validation report. We found that it is more or less consistent with the previous comparison studies such as Schneider et al. (2005); Viatte et al. (2011).

There are possible reasons that have been suggested for the differences between FTIR and satellite measurements during comparison. Tropics are well characterized by





AMTD
5, 6763–6812, 2012



strong dynamics so that it could contribute for the discrepancy of the comparisons. As reported by Ture (2011), there is also strong interaction between tropics and midlatitude as well as stratosphere-troposphere exchange during Rossby wave breaking bringing in rich ozone airmass into the tropics. The other factor for the discrepancy among instruments comparisons is due to inconsistencies in the spectroscopic parameters such as UV and IR spectroscopy of ozone.

*Acknowledgements.* We are grateful to the Goddard Space Flight Center for providing temperature and pressure profiles via automailer system. We are greatly acknowledge the MLS, MIPAS, TES, OMI, AIRS and GOME science teams for the satellite data used in this study. Finally, author would like to thank Samara university for the sponsorship.

## References

Balis, D., Kroon, M., Koukouli, M. E., Brinksma, E. J., Labow, G., Veefkind, J. P., and McPeters, R. D.: Validation of ozone monitoring instrument total ozone column measurements using Brewer and Dobson spectrophotometer ground-based observations, J. Geophys. Res., 112, D24S46, doi:10.1029/2007JD008796, 2007a. 6775

Balis, D., Lambert, J. C., Van Roozendael, M., Spurr, R., Loyola, D., Livschitz, Y., Valks, P., Amiridis, V., Gerard, P., Granville, J., and Zehner, C.: Ten years of GOME/ERS2 total ozone data the new GOME data processor (GDP) version 4.2: Ground-based validation and comparisons with TOMS V7/V8, J. Geophys. Res., 112, D07307, doi:10.1029/2005JD006376, 2007b.

Balis, D., Koukouli, M., Loyola, D., Valks, P., and Hao, N.: Second validation report of GOME-2 total ozone products (OTO/O3, NTO/O3) processed with GDP4.2, Report of the Satellite Application Facility on Ozone and Atmospheric Chemistry Monitoring (O3M-SAF), SAF/O3M/AUTH/GOME-2VAL/RP/02, 2008.

Barret, B., De Maziére, M., and Demoulin, P.: Retrieval and characterization of ozone profiles from solar infrared spectra at the Jungfraujoch: J. Geophys. Res., 107, 4788, doi:10.1029/2001JD001298, 2002.





AMTD

5, 6763–6812, 2012



Barret, B., De Maziére, M., and Demoulin, P.: Correction to "Retrieval and characterization of ozone profiles from solar infrared spectra at the Jungfraujoch", J. Geophys. Res., 108, 4372, doi:10.1029/2003JD003809, 2003.

Beer, R., Glavich, T., and Rider, D.: Tropospheric emission spectrometer for the earth observing systems Aura satellite, Appl. Optics, 40, 2356–2367, 2001.

Bowman, K. W., Worden, J., Steck, T., Worden, H. M., Clough, S., and Rodgers, C.: Capturing time and vertical variability of tropospheric ozone: a study using TES nadir retrievals, J. Geophys. Res., 107, 4723, doi:10.1029/2002JD002150, 2002.

Bowman, K. W., Rodgers, C. D., Sund-Kulawik, S., Worden, J., Sarkissian, E., Osterman, G., Steck, T., Luo, M., Eldering, A., Shephard, M. W., Worden, H., Clough, S. A., Brown, P. D., Rinsland, C. P., Lampel, M., Gunson, M., and Beer, R.: Tropospheric emission spectrometer: retrieval method and error analysis, IEEE T. Geosci. Remote, 44, 1295–1307, 2006.

Chauhan, S., Höpfner, M., Stiller, G. P., von Clarmann, T., Funke, B., Glatthor, N., Grabowski, U., Linden, A., Kellmann, S., Milz, M., Steck, T., Fischer, H., Froidevaux, L., Lambert, A., Santee, M. L., Schwartz, M., Read, W. G., and Livesey, N. J.: MIPAS reduced spectral resolution UTLS-1 mode measurements of temperature, $O_3$, $HNO_3$, $N_2O$, $H_2O$ and relative humidity over ice: retrievals and comparison to MLS, Atmos. Meas. Tech., 2, 337–353, doi:10.5194/amt-2-337-2009, 2009.

Clough, S. A., Worden, J. R., Brown, P. D., Shephard, M. W., Rinsland, C. P., and Beer, R.: Retrieval of tropospheric ozone from simulations of nadir spectral radiances from space, J. Geophys. Res., 107, 4589, doi:10.1029/2001JD001307, 2002.

Cofield, R. E. and Stek, P. C.: Design and field-of-view calibration of 114660 GHz optics of the earth observing system microwave limb sounder, IEEE T. Geosci. Remote Sens., 44, 1166–1181, doi:10.1109/TGRS.2006.873234, 2006.

Dupuy, E., Walker, K. A., Kar, J., Boone, C. D., McElroy, C. T., Bernath, P. F., Drummond, J. R., Skelton, R., McLeod, S. D., Hughes, R. C., Nowlan, C. R., Dufour, D. G., Zou, J., Nichitiu, F., Strong, K., Baron, P., Bevilacqua, R. M., Blumenstock, T., Bodeker, G. E., Borsdorff, T., Bourassa, A. E., Bovensmann, H., Boyd, I. S., Bracher, A., Brogniez, C., Burrows, J. P., Catoire, V., Ceccherini, S., Chabrillat, S., Christensen, T., Coffey, M. T., Cortesi, U., Davies, J., De Clercq, C., Degenstein, D. A., De Mazière, M., Demoulin, P., Dodion, J., Firanski, B., Fischer, H., Forbes, G., Froidevaux, L., Fussen, D., Gerard, P., Godin-Beekmann, S., Goutail, F., Granville, J., Griffith, D., Haley, C. S., Hannigan, J. W., Höpfner, M., Jin, J. J., Jones, A., Jones, N. B., Jucks, K., Kagawa, A., Kasai, Y., Kerzenmacher, T. E., Kleinböhl, A.,





AMTD
5, 6763–6812, 2012



Klekociuk, A. R., Kramer, I., Küllmann, H., Kuttippurath, J., Kyrölä, E., Lambert, J.-C., Livesey, N. J., Llewellyn, E. J., Lloyd, N. D., Mahieu, E., Manney, G. L., Marshall, B. T., McConnell, J. C., McCormick, M. P., McDermid, I. S., McHugh, M., McLinden, C. A., Mellqvist, J., Mizutani, K., Murayama, Y., Murtagh, D. P., Oelhaf, H., Parrish, A., Petelina, S. V., Piccolo, C., Pommereau, J.-P., Randall, C. E., Robert, C., Roth, C., Schneider, M., Senten, C., Steck, T., Strandberg, A., Strawbridge, K. B., Sussmann, R., Swart, D. P. J., Tarasick, D. W., Taylor, J. R., Tétard, C., Thomason, L. W., Thompson, A. M., Tully, M. B., Urban, J., Vanhellemont, F., Vigouroux, C., von Clarmann, T., von der Gathen, P., von Savigny, C., Waters, J. W., Witte, J. C., Wolff, M., and Zawodny, J. M.: Validation of ozone measurements from the Atmospheric Chemistry Experiment (ACE), Atmos. Chem. Phys., 9, 287–343, doi:10.5194/acp-9-287-2009, 2009.

Fischer, H., Birk, M., Blom, C., Carli, B., Carlotti, M., von Clarmann, T., Delbouille, L., Dudhia, A., Ehhalt, D., Endemann, M., Flaud, J. M., Gessner, R., Kleinert, A., Koopman, R., Langen, J., López-Puertas, M., Mosner, P., Nett, H., Oelhaf, H., Perron, G., Remedios, J., Ridolfi, M., Stiller, G., and Zander, R.: MIPAS: an instrument for atmospheric and climate research, Atmos. Chem. Phys., 8, 2151–2188, doi:10.5194/acp-8-2151-2008, 2008.

Froidevaux, L., Livesey, N. J., Read, W. G., Jiang, Y. B., Jimenez, C., Filipiak, M. J., Schwartz, M. J., Santee, M. L., Pumphrey, H. C., Jiang, J. H., Wu, D. L., Manney, G. L., Drouin, B. J., Waters, J. W., Fetzer, E. J., Bernath, P. F., Boone, C. D., Walker, K. A., Jucks, K. W., Toon, G. C., Margitan, J. J., Sen, B., Webster, C. R., Christensen, L. E., Elkins, J. W., Atlas, E., Lueb, R. A., and Hendershot, R.: Early Validation Analyses of Atmospheric Profiles From EOS MLS on the Aura Satellite, IEEE T. Geosci. Remote, 44, 1106–1121, 2006.

Froidevaux, L., Jiang, Y. B., Lambert, A., Livesey, N. J., Read, W. G., Waters, J. W., Browell, E. V., Hair, J. W., Avery, M. A., McGee, T. J., Twigg, L. W., Sumnicht, G. K., Jucks, K. W., Margitan, J. J., Sen, B., Stachnik, R. A., Toon, G. C., Bernath, P. F., Boone, C. D., Walker, K. A., Filipiak, M. J., Harwood, R. S., Fuller, R. A., Manney, G. L., Schwartz, M. J., Daffer, W. H., Drouin, B. J., Cofield, R. E., Cuddy, D. T., Jarnot, R. F., Knosp, B. W., Perun, V. S., Snyder, W. V., Stek, P. C., Thurstans, R. P., and Wagner, P. A.: Validation of Aura Microwave Limb Sounder stratospheric ozone measurements, J. Geophys. Res., 113, D15S20, doi:10.1029/2007JD008771, 2008.

Funke, B. and von Clarmann, T.: How to average logarithmic retrievals?, Atmos. Meas. Tech., 5, 831–841, doi:10.5194/amt-5-831-2012, 2012.





AMTD
5, 6763–6812, 2012



Griesfeller, A., Griesfeller, J., Hase, F., Krammer, I., Loes, P., Mikuteit, S., Raffalski, U., Blumentstock, T., and Nakajima, H.: Comparison of ILAS-II and ground-based FTIR measurements of $O_3$, $HNO_3$, $N_2$, and $CH_4$ over Kiruna, Sweden, J. Geophys. Res., 111, D11S07, doi:10.1029/2005JD006451, 2006. 6785

Hase, F., Blumenstock, T., and Paton-Walsh, C.: Analysis of the instrumental line shape of high-resolution Fourier transform IR spectrometers with gas cell measurements and new retrieval software, Appl. Optics, 38, 3417–3422, 1999. 6768

Hase, F., Hannigan, J. W., Coffey, M. T., Goldman, A., Hopfner, M., Jones, N. B., Rinsland, C. P., and Wood, S. W.: Intercomparison of retrieval codes used for the analysis of high-resolution, ground-based FTIR measurements, J. Quant. Spectrosc. Ra., 87, 25–52, 2004. 6767

Holton, J. R.: Introduction to dynamic meteorology, 4th Edn., Department of Atmospheric Sciences University of Washington, Elsevier Academic Press, 2004.

Hoogen, R., Rozanov, V. V., and Burrows, J. P.: Ozone profiles from GOME satellite data: algorithm description and first validation, J. Geophys. Res., 104, 8263–8280, 1999.

Intergovernmental Panel on Climate Change (IPCC): Climate Change 2007: The Physical Science Basis, Contribution of Working Group I to the Fourth Assessment Report of the Intergovernmental Panel on Climate Change, edited by: Solomon, S., Qin, D., Manning, M., Chen, Z., Marquis, M., Averyt, K. B., Tignor, M., and Miller, H. L., Cambridge University Press, Cambridge, UK and New York, NY, USA, 996 pp., 2007.

Jarnot, R. F., Perun, V. S., and Schwartz, M. J.: Radiometric and spectral performance and calibration of the GHz bands of EOS MLS, IEEE T. Geosci. Remote, 44, 1131–1143, doi:10.1109/TGRS.2005.863714, 2006.

Jiang, Y. B., Froidevaux, L., Lambert, A., Livesey, N. J., Read, W. G., Waters, J. W., Bojkov, B., Leblanc, T., McDermid, I. S., Godin-Beekmann, S., Filipiak, M. J., Harwood, R. S., Fuller, R. A., Daffer, W. H., Drouin, B. J., Cofield, R. E., Cuddy, D. T., Jarnot, R. F., Knosp, B. W., Perun, V. S., Schwartz, M. J., Snyder, W. V., Stek, P. C., Thurstans, R. P., Wagner, P. A., Allaart, M., Andersen, S. B., Bodeker, G., Calpini, B., Claude, H., Coetzee, G., Davies, J., De Backer, H., Dier, H., Fujiwara, M., Johnson, B., Kelder, H., Leme, N. P., Konig-Langlo, G., Kyro, E., Laneve, G., Fook, L. S., Merrill, J., Morris, G., Newchurch, M., Oltmans, S., Parrondos, M. C., Posny, F., Schmidlin, F., Skrivankova, P., Stubi, R., Tarasick, D., Thompson, A., Thouret, V., Viatte, P., Vomel, H., von Der Gathen, P., Yela, M., and Zablocki, G.: Validation of aura microwave limb sounder ozone by ozonesonde and lidar measurements, J. Geophys. Res., 112, D24S34, doi:10.1029/2007JD008776, 2007.





AMTD
5, 6763–6812, 2012



Jacobson, M. Z.: Fundamentals of Atmospheric Modeling, 2nd edn., Stanford University, Cambridge University press, 2005.

Levelt, P. F., van der A, R. J., Bhartia, P. K., Boersma, F., Brinksma, E., Carpay, J., Chance, K., de Haan, J., Hilsenrath, E., Isaksen, I., Kelder, H., Leppelmeier, G. W., Malkki, A., McPeters, R. D., Noordhoek, R., van den Oord, G. H. J., van Oss, R., Piters, A., Snel, R., Stammes, P., Valks, P., Veefkind, J. P., van Velthoven, P., Voors, R., and van Weele, M.: Science Requirements Document for OMI-EOS, RS-OMIE-KNMI-001, 2000. 6775

Levelt, P. F., van den Oord, G. H. J., Dobber, M. R., Malkki, A., Visser, H., de Vries, J., Stammes, P., Lundell, J. O. V., and Saari, H.: The ozone monitoring instrument, IEEE T. Geosci. Remote, 44, 1093–1101, 2006. 6774

Lindenmaier, R., Batchelor, R. L., Strong, K., Fast, H, Goutail, F., Kolonjari, F., McElroy, C. T., Mittermeier, R. L., and Walker, K. A.: An evaluation of infrared microwindows for ozone retrievals using the Eureka Bruker 125HR Fourier transform spectrometer, J. Quant. Spectrosc. Ra., 111, 569–585, 2010.

Liu, X., Bhartia, P. K., Chance, K., Froidevaux, L., Spurr, R. J. D., and Kurosu, T. P.: Validation of Ozone Monitoring Instrument (OMI) ozone profiles and stratospheric ozone columns with Microwave Limb Sounder (MLS) measurements, Atmos. Chem. Phys., 10, 2539–2549, doi:10.5194/acp-10-2539-2010, 2010. 6775

Livesey, N. J., Van Snyder, W., Read, W. J., and Wagner, P. A.: Retrieval algorithms for the EOS Microwave Limb Sounder (MLS), IEEE T. Geosci. Remote, 44, 1144–1155, doi:10.1109/TGRS.2006.872327, 2006.

Livesey, N. J., Filipiak, M. J., Froidevaux, L., Read, W. G., Lambert, A., Santee, M. L., Jiang, J. H., Pumphrey, H. C., Waters, J. W., Cofield, R. E., Cuddy, D. T., Daffer, W. H., Drouin, B. J., Fuller, R. A., Jarnot, R. F., Jiang, Y. B., Knosp, B. W., Li, Q. B., Perun, V. S., Schwartz, M. J., Snyder, W. V., Stek, P. C., Thurstans, R. P., Wagner, P. A., Avery, M., Browell, E. V., Cammas, J. P., Christensen, L. E., Diskin, G. S., Gao, R. S., Jost, H. J., Loewenstein, M., Lopez, J. D., Nedelec, P., Osterman, G. B., Sachse, G. W., and Webster, C. R.: Validation of aura microwave limb sounder $O_3$ and CO observations in the upper troposphere and lower stratosphere, J. Geophys. Res., 113, D15S02, doi:10.1029/2007JD008805, 2008.

Lucke, R. L., Korwan, D., Bevilacqua, R. M., Hornstein, J. S., Shettle, E. P., Chen, D. T., Daehler, M., Lumpe, J. D., Fromm, M. D., Debrestian, D., Neff, B., Squire, M., König-Langlo, G., and Davies, J.: The Polar Ozone and Aerosol Measurement (POAM III) instrument and early validation results, J. Geophys. Res., 104, 18785–18799, 1999.





AMTD
5, 6763–6812, 2012



Mengistu Tsidu, G.: The role of chemistry and transport on $NO_y$ partitioning and budget during Austral Spring 2002 as derived from MIPAS measurement, PhD dissertation, Institut für Meteorologie und Klimaforschung, Germany, 2005.
Nassar, R., Logan, J. A., Worden, H. M., Megretskaia, I. A., Bowman, K. W., Osterman, G. B., Thompson, A. M., Tarasick, D. W., Austin, S., Claude, H., Dubey, M. K., Hocking, W. K., Johnson, B. J., Joseph, E., Merrill, J., Morris, G. A., Newchurch, M., Oltmans, S. J., Posny, F., Schmidlin, F. J., Vomel, H., Whiteman, D. N., and Witte, J. C.: Validation of Tropospheric Emission Spectrometre (TES) nadir ozone profiles using ozonesonde measurements, J. Geophys. Res., 113, D15S17, doi:10.1029/2007JD008819, 2008.
Phillips, D.: A technique for the numerical solution of certain integral equations of first kind, J. Assoc. Comput. March., 9, 84–97, 1962.
Pickett, H. M.: Microwave limb sounder THz module on Aura, IEE E. Trans. Geosci. Remote Sens., 44, 1122–1130, 2006.
Platt, U.: Differential optical absorption spectroscopy (DOAS), in: Air Monitoring by Spectroscopic Techniques, John Wiley, New York, 8427, 1994. 6776
Richards, N., Osterman, G. B., Browell, E. V., Hair, J., Avery, A., and Li, Q. B.: Validation of Tropospheric Emission Spectrometre (TES) ozone profiles with aircraft observations during INTEX-B, J. Geophys. Res., 113, D16S29, doi:10.1029/2007JD008815, 2008.
Rodgers, C. D.: Retrieval of atmospheric temperature and composition from remote measurements of thermal radiation, Rev. Geophys., 14, 609–624, 1976.
Rodgers, C. D.: Inverse methods for atmospheric sounding theory and practise, in: Series on Atmospheric, Oceanic and Planetary Physics, Vol. 2, World Scientific, 2000.
Rodgers, C. D. and Connor, B. J.: Intercomparison of remote sounding instruments, J. Geophys. Res., 108, 4116, doi:10.1029/2002JD002299, 2003.
Rothman, L. S., Jacquemart, D., Barbe, A., Chris Bennerc, D., Birk, M., Brown, L. R., Carleer, M. R., Chackerian Jr., C., Chance, K., Coudert, L. H., Dana, V., Devi, V. M., Flaud, J.-M., Gamache, R. R., Goldman, A., Hartmann, J.-M., Jucks, K. W., Maki, A. G., Mandin, J.-Y., Massie, S. T., Orphal, J., Perrin, A., Rinsland, C. P., Smith, M. A. H., Tennyson, J., Tolchenov, R. N., Toth, R. A., Vander Auwera, J., Varanasi, P., and Wagner, G.: The HITRAN 2004 molecular spectroscopic database, J. Quant. Spectrosc. Ra., 96, 139–204, 2005. 6767
Schneider, M.: Continuous observations of atmospheric trace gases by ground-based FTIR spectroscopy at Izana observatory, Tenerife Island, PhD dissertation, at Institute of Metrology and Klimaforschung, 2002.





AMTD
5, 6763–6812, 2012



Schneider, M., Blumenstock, T., Hase, F., Höpfner, M., Cuevas, E., Redondas, A., and Sancho, J. M.: Ozone profiles and total column amounts drived at Izaña, Tenerife Island, from FTIR solar absorption spectra, and its validation by intercomparision to ECC-sonde and Brewer spectrometer measurements, J. Quant. Spectrosc. Ra., 91, 245–274, 2005.

Schneider, M., Hase, F., and Blumenstock, T.: Water vapour profiles by ground-based FTIR spectroscopy: study for an optimised retrieval and its validation, Atmos. Chem. Phys., 6, 811–830, doi:10.5194/acp-6-811-2006, 2006.

Schoeberl, M. R., Douglass, A. R., Hilsenrath, E., Bhartia, P. K., Beer, R., Waters, J. W., Gunson, M. R., Froidevaux, L., Gille, J. C., Barnett, J. J., Levelt, P. F., and DeCola, P.: Overview of the EOS Aura mission, IEEE T. Geosci. Remote, 44, 1066–1074, 2006.

Senten, C., De Mazière, M., Dils, B., Hermans, C., Kruglanski, M., Neefs, E., Scolas, F., Vandaele, A. C., Vanhaelewyn, G., Vigouroux, C., Carleer, M., Coheur, P. F., Fally, S., Barret, B., Baray, J. L., Delmas, R., Leveau, J., Metzger, J. M., Mahieu, E., Boone, C., Walker, K. A., Bernath, P. F., and Strong, K.: Technical Note: New ground-based FTIR measurements at Ile de La Réunion: observations, error analysis, and comparisons with independent data, Atmos. Chem. Phys., 8, 3483–3508, doi:10.5194/acp-8-3483-2008, 2008. 6780

Shavrinam, A. V., Pavlenko, Y. V., Veles, A., Syniavskyi, I., and Kroon, M.: Ozone columns obtained by ground-based remote sensing in Kiev for Aura Ozone Measuring Instrument validation, J. Geophys. Res., 112, D24S45, doi:10.1029/2007JD008787, 2007.

Seinfeld, J. H. and Pandis, S. N; Atmospheric Chemistry and Physics: from Air Pollution to Climate Change, 2nd Edn., John Wiley and Sons, Inc., 2006. 6765

Steck, T., von Clarmann, T., Fischer, H., Funke, B., Glatthor, N., Grabowski, U., Höpfner, M., Kellmann, S., Kiefer, M., Linden, A., Milz, M., Stiller, G. P., Wang, D. Y., Allaart, M., Blumenstock, Th., von der Gathen, P., Hansen, G., Hase, F., Hochschild, G., Kopp, G., Kyrö, E., Oelhaf, H., Raffalski, U., Redondas Marrero, A., Remsberg, E., Russell III, J., Stebel, K., Steinbrecht, W., Wetzel, G., Yela, M., and Zhang, G.: Bias determination and precision validation of ozone profiles from MIPAS-Envisat retrieved with the IMK-IAA processor, Atmos. Chem. Phys., 7, 3639–3662, doi:10.5194/acp-7-3639-2007, 2007.

Stiller, G. P., Kiefer, M., Eckert, E., von Clarmann, T., Kellmann, S., García-Comas, M., Funke, B., Leblanc, T., Fetzer, E., Froidevaux, L., Gomez, M., Hall, E., Hurst, D., Jordan, A., Kämpfer, N., Lambert, A., McDermid, I. S., McGee, T., Miloshevich, L., Nedoluha, G., Read, W., Schneider, M., Schwartz, M., Straub, C., Toon, G., Twigg, L. W., Walker, K., and Whiteman, D. N.: Validation of MIPAS IMK/IAA temperature, water vapor, and ozone





AMTD
5, 6763–6812, 2012



profiles with MOHAVE-2009 campaign measurements, Atmos. Meas. Tech., 5, 289–320, doi:10.5194/amt-5-289-2012, 2012.
Strow, L. L., Hannon S. E., de Souza-Machado, S., Motteler, H. E., and Tobin, D.: An Overview of the AIRS Radiative Transfer Model, IEEE T. Geosci. Remote, 41, 303–313, 2003. 6776
Tikhonov, A.: On the solution of incorrectly stated problems and method of regularization, Dokl. Akad, Nauk. SSSR, 151, 501–504, 1963.
Ture, K.: Ozone dynamics and seasonal variability over Africa, PhD dissertation, Addis Ababa University, Ethiopia, 2011.
Van Roozendael, M., Lambert, J. C., Spurr, R. J. D., and Fayt, C.: GOME Direct Fitting (GODFIT) GDOAS Delta Validation Report, ERS Exploitation AO/1-4235/02/I-LG, Oberpfaffenhofen, Germany, 2004. 6777
Van Roozendael, M., Loyola, D., Spurr, R., Balis, D., Lambert, J.-C., Livschitz, Y., Valks, P., Ruppert, T., Kenter, P., Fayt, C., and Zehner, C.: Reprocessing the 10-year GOME/ERS-2 total ozone record for trend analysis: the new GOME Data Processor Version 4.0, Algorithm Description, J. Geophys. Res., 111, D14311, doi:10.1029/2005JD006375, 2006. 6776
Viatte, C., Schneider, M., Redondas, A., Hase, F., Eremenko, M., Chelin, P., Flaud, J.-M., Blumenstock, T., and Orphal, J.: Comparison of ground-based FTIR and Brewer $O_3$ total column with data from two different IASI algorithms and from OMI and GOME-2 satellite instruments, Atmos. Meas. Tech., 4, 535–546, doi:10.5194/amt-4-535-2011, 2011. 6784
Vigouroux, C., De Mazière, M., Errera, Q., Chabrillat, S., Mahieu, E., Duchatelet, P., Wood, S., Smale, D., Mikuteit, S., Blumenstock, T., Hase, F., and Jones, N.: Comparisons between ground-based FTIR and MIPAS $N_2O$ and $HNO_3$ profiles before and after assimilation in BASCOE, Atmos. Chem. Phys., 7, 377–396, doi:10.5194/acp-7-377-2007, 2007. 6768
von Clarmann, T., Höpfner, M., Kellmann, S., Linden, A., Chauhan, S., Funke, B., Grabowski, U., Glatthor, N., Kiefer, M., Schieferdecker, T., Stiller, G. P., and Versick, S.: Retrieval of temperature, $H_2O$, $O_3$, $HNO_3$, $CH_4$, $N_2O$, $ClONO_2$ and ClO from MIPAS reduced resolution nominal mode limb emission measurements, Atmos. Meas. Tech., 2, 159–175, doi:10.5194/amt-2-159-2009, 2009.
WMO (World Meteorological Organization): Scientific assessment of ozone depletion: 2006, WMO Global Ozone Res. and Monit. Project, Rep. 50, World Meteorol. Org., Geneva, 2007. 6765
Worden, H. M., Logan, J. A., Worden, J. R., Beer, R., Bowman, K., Clough, S. A., Eldering, A., Fisher, B. M., Gunson, M. R., Herman, R. L., Kulawik, S. S., Lampel, M. C., Luo, M., Megret-





AMTD
5, 6763–6812, 2012



skaia, I. A., Osterman, G. B., and Shephard, M. W.: Comparisons of Tropospheric Emission Spectrometer (TES) ozone profiles to ozonesondes: methods and initial results, J. Geophys. Res., 112, D03309, doi:10.1029/2006JD007258, 2007.

Worden, J., Kulawik, S. S., Shepard, M., Clough, S., Worden, H., Bowman, K., and Goldman, A.: Predicted errors of tropospheric emission spectrometer nadir retrievals from spectral window selection, J. Geophys. Res., 109, D09308, doi:10.1029/2004JD004522, 2004.

Wunch, D., Taylor, J. R., Fu, D., Bernath, P., Drummond, J. R., Midwinter, C., Strong, K., and Walker, K. A.: Simultaneous ground-based observations of $O_3$, HCl, $N_2O$, and $CH_4$ over Toronto, Canada by three Fourier transform spectrometers with different resolutions, Atmos. Chem. Phys., 7, 1275–1292, doi:10.5194/acp-7-1275-2007, 2007.

Young-In Won: Document for AIRS level-3 Version 5 Standard Products, GES DISC, 3 March, 2008.

Zhang, L., Jacob, D. J., Liu, X., Logan, J. A., Chance, K., Eldering, A., and Bojkov, B. R.: Intercomparison methods for satellite measurements of atmospheric composition: application to tropospheric ozone from TES and OMI, Atmos. Chem. Phys. Discuss., 10, 1417–1456, doi:10.5194/acpd-10-1417-2010, 2010.





AMTD
5, 6763–6812, 2012



**Table 1.** Summary of the characteristics of the instruments and measurement systems of $O_3$ addressed in this study.

| Instrumets | FTIR | MLS | MIPAS | TES | OMI | AIRS | GOME-2 |
|---|---|---|---|---|---|---|---|
| Platform | Ground-based | Satellite | Satellite | Satellite | Satellite | Satellite | Satellite |
| Observation geometry | upward | limb | limb | nadir | nadir | nadir | nadir |
| Observation mode | absorption | emission | emission | emission | back-scattered | emission | back-scattered |
| Vertical resolution (km) | ~ 9–15 | 3–4 | 3.5–5 | ~ 6 | 3–5 | greater than ~ 6 | 3–5 |
| Spectral resolution | 0.009 $cm^{-1}$ | | 0.0625 $cm^{-1}$ | 0.1 $cm^{-1}$ | 0.42–0.63 nm | 0.5–2 $cm^{-1}$ | ~ 0.24 nm |
| Spectral domain | 600–4400 $cm^{-1}$ | ~ 80,000 $cm^{-1}$ (~ 240 GHz) | 685 2410 $cm^{-1}$ | 650–2250 $cm^{-1}$ | 270–330 nm | 650–2700 $cm^{-1}$ | 325–335 nm |





AMTD
5, 6763–6812, 2012



**Table 2.** Summary of the comparison between $O_3$ columns amount derived from FTIR and from various satellites data (MLS, TES, OMI, AIRS and GOME-2) over Addis Ababa. *N* represents number of coincidences.

| Comparison of FTIR with | *N* | Mean Relative Difference (%) |
|---|---|---|
| MLS | 76 | $3.9 \pm 4.3$ |
| TES | 13 | $-2.6 \pm 10.5$ |
| OMI | 70 | $-0.4 \pm 6.3$ |
| AIRS | 70 | $-6.8 \pm 7.6$ |
| GOME-2 | 46 | $0.5 \pm 2.2$ |





AMTD
5, 6763–6812, 2012



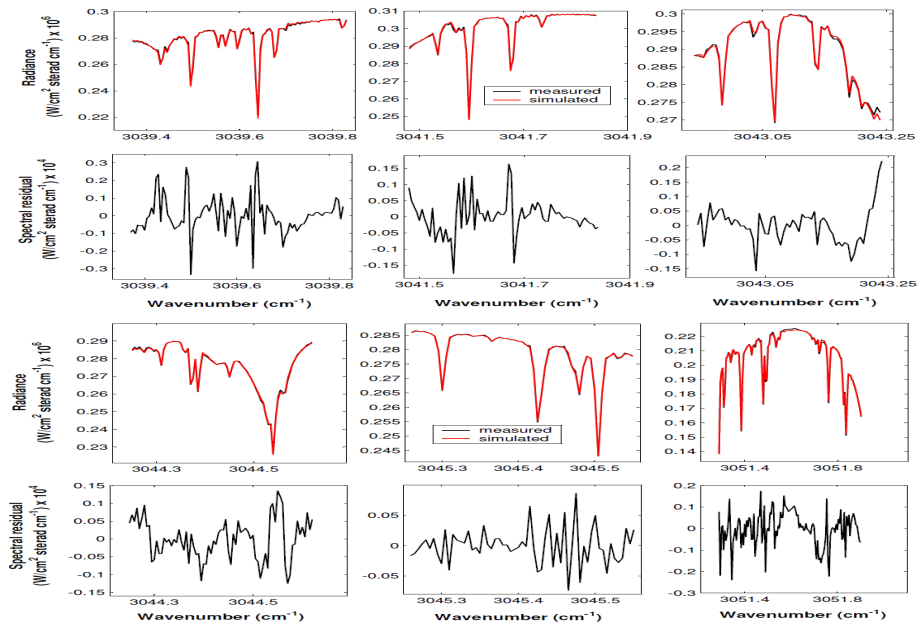


**Fig. 1.** $O_3$ – the top and the third panels show the measured spectrum (black line) and simulated spectrum (red line); and the second and the bottom panels show spectral residuals on 27 May 2010.





AMTD
5, 6763–6812, 2012

Retrieval and validation of $O_3$ from FTIR observation

S. Takele Kenea et al.



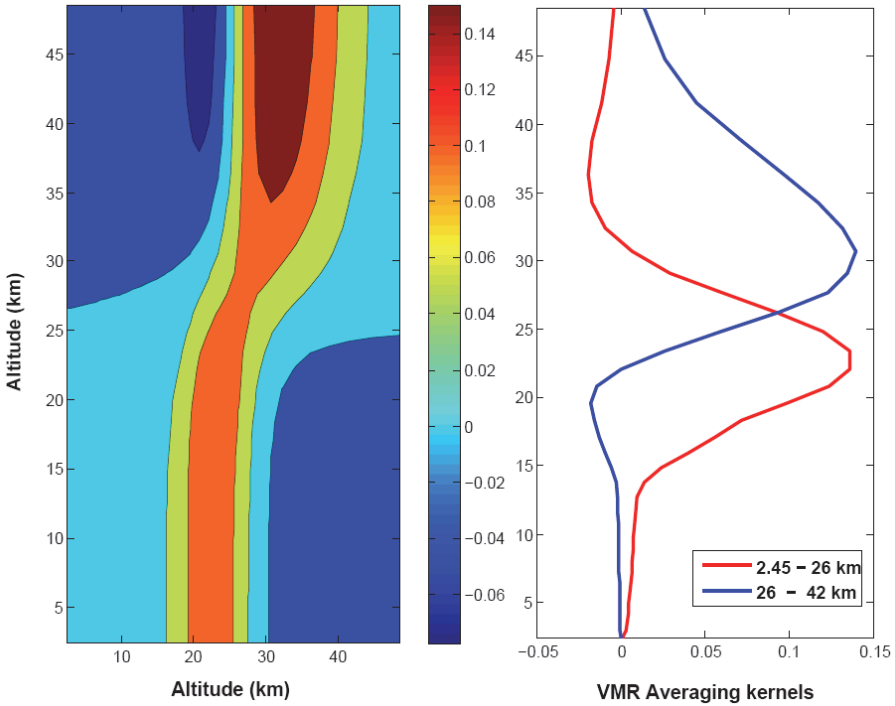


**Fig. 2.** The left panels show averaging kernels matrix plot and the right panels depict volume mixing ratio averaging kernels (ppmv/ppmv) for the altitude ranges listed in the legend for $O_3$ on 27 May 2010.





AMTD
5, 6763–6812, 2012



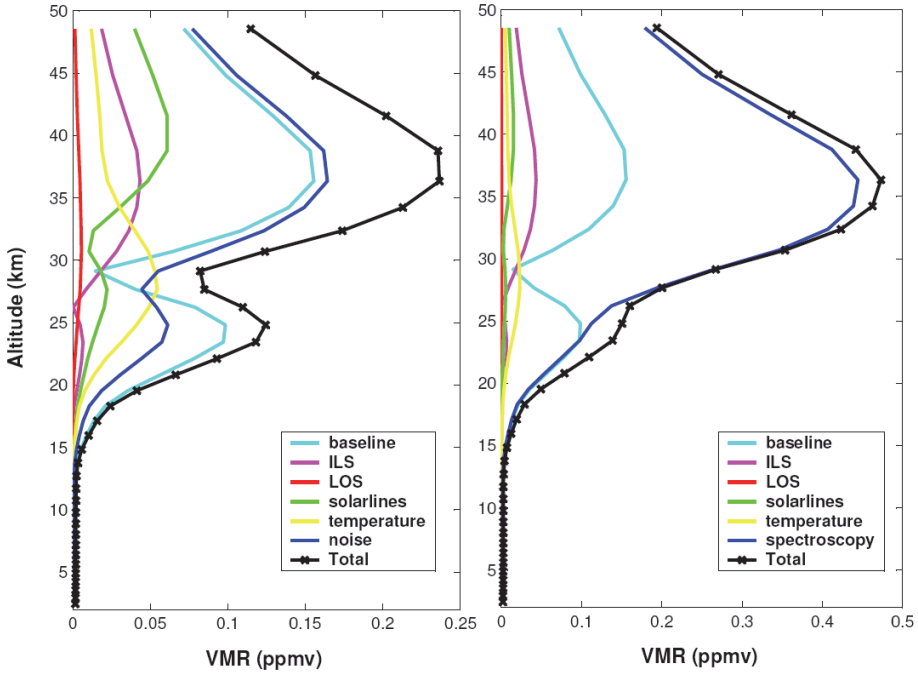


**Fig. 3.** FTIR error analysis: estimated uncertainty profiles for statistical (left-panel) and systematic (right-panel) contributions.





AMTD
5, 6763–6812, 2012



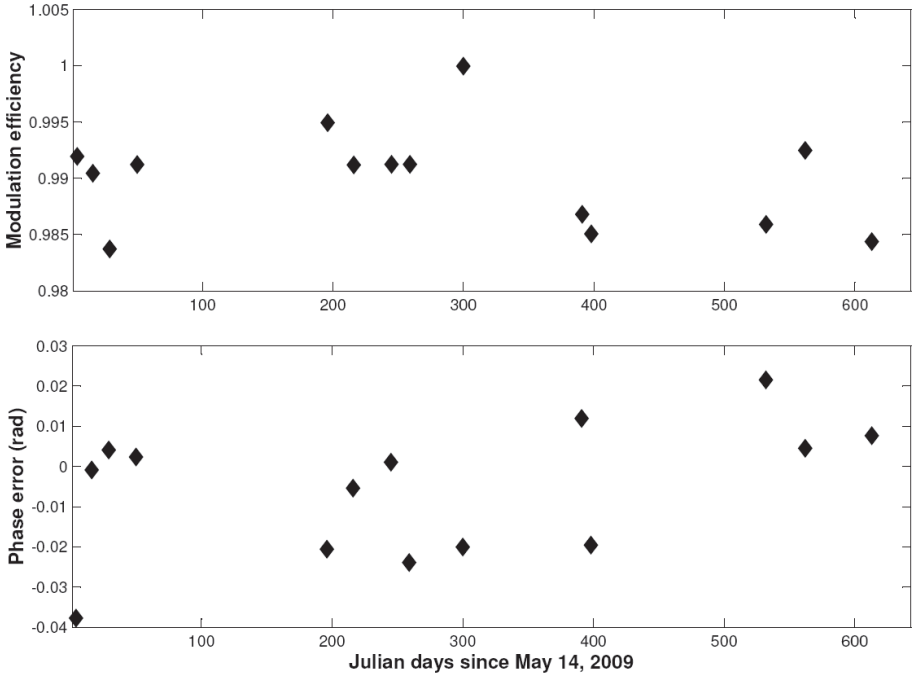


**Fig. 4.** Evolution of the ILS during the measurement period.





AMTD
5, 6763–6812, 2012



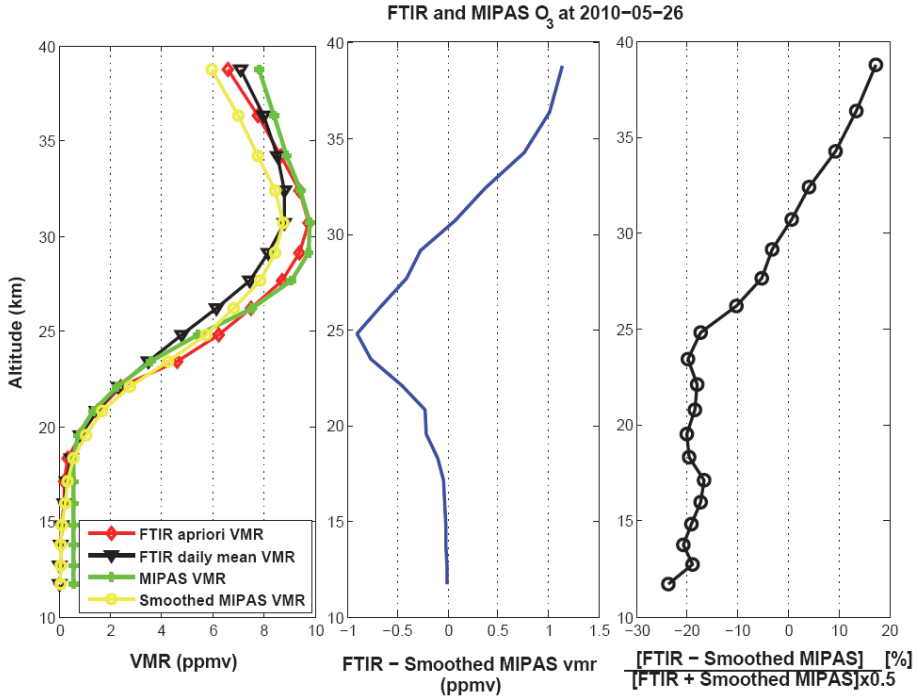


**Fig. 5.** Comparisons of $O_3$ VMR profiles from the FTIR and MLS at Addis Ababa on 27 May 2010. On the left panel: $O_3$ VMR profiles of FTIR apriori (red with diamond symbol), FTIR daily mean (black with triangle symbol), MLS smoothed (yellow with circle) and MLS (green with plus sign symbol), as function of altitude. Differences between the FTIR and smoothed MLS are shown with units of volume mixing ratio and % (solid line with circle) on the middle and right panels respectively.





AMTD
5, 6763–6812, 2012



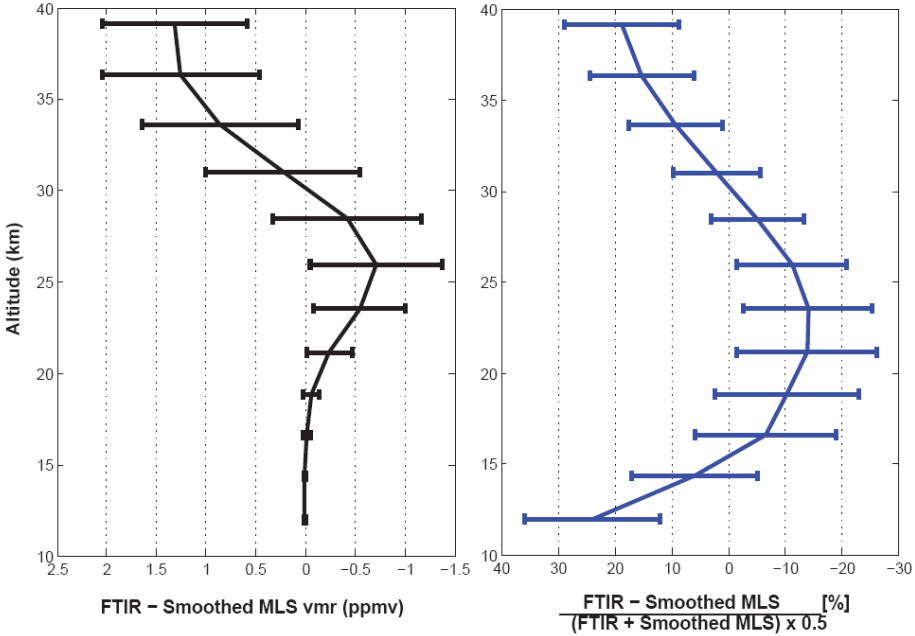


**Fig. 6.** Statistics for 76 matched $O_3$ VMR profiles from FTIR and smoothed MLS measurements at Addis Ababa. Means of the differences and standard deviations are shown.





AMTD
5, 6763–6812, 2012



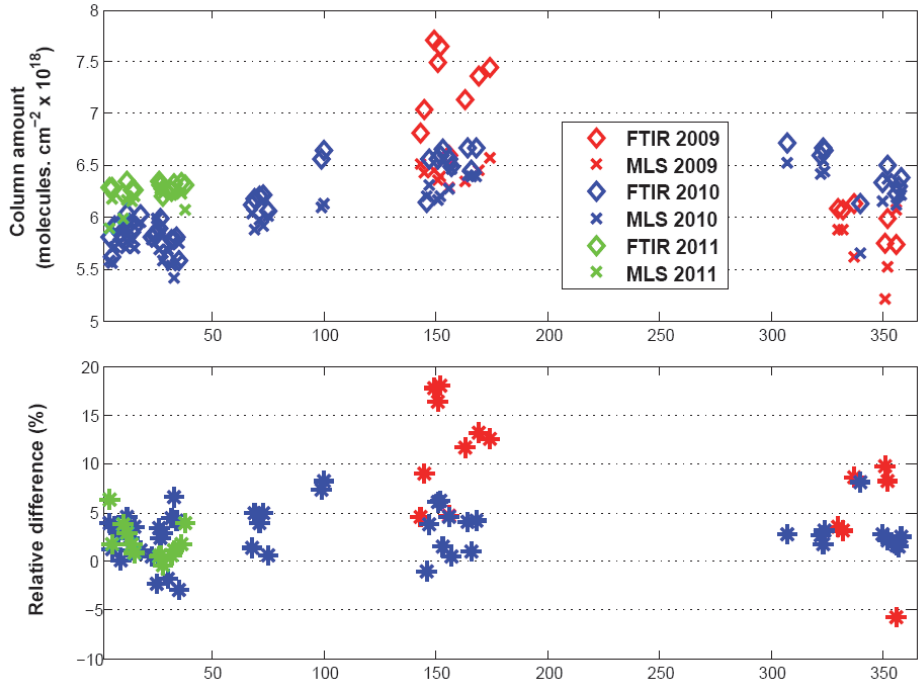


**Fig. 7.** The top panel shows the stratospheric column values $O_3$ for FTIR (open diamonds) and for the correlative MLS measurements (cross). The bottom panel gives the relative differences between the stratospheric column values of FTIR and MLS (for 76 coincident measurements).





AMTD
5, 6763–6812, 2012



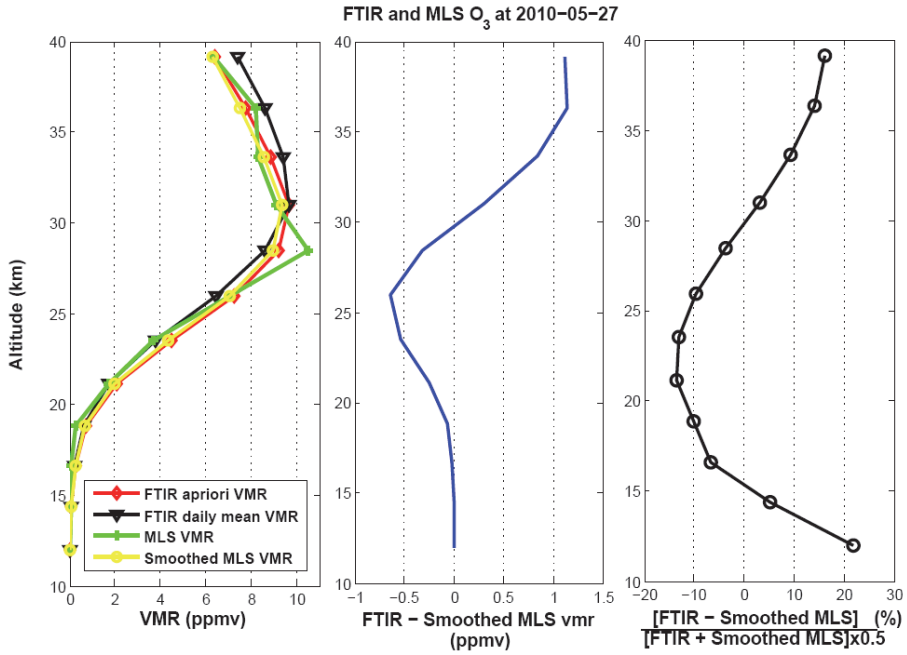


**Fig. 8.** Comparisons of $O_3$ VMR profiles from the FTIR and MIPAS at Addis Ababa on 26 May 2010. On the left panel: $O_3$ VMR profiles of FTIR apriori (red with diamond symbol), FTIR daily mean (black with triangle symbol), MIPAS smoothed (yellow with circle) and MIPAS (green with plus sign symbol), as function of altitude. Differences between the FTIR and smoothed MIPAS are shown with units of volume mixing ratio and % (solid line with circle) on the middle and right panels respectively.





AMTD
5, 6763–6812, 2012



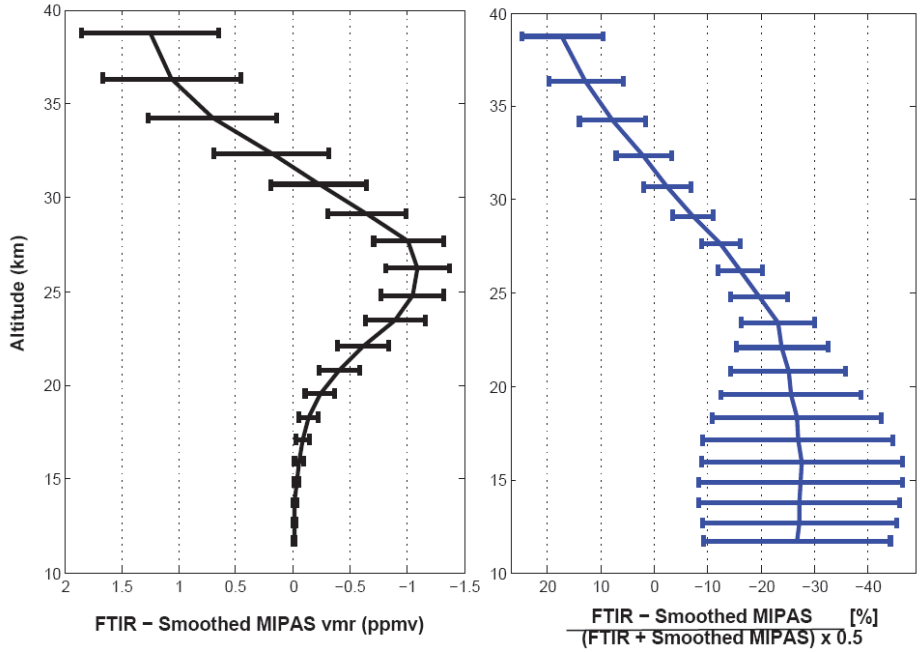


**Fig. 9.** Statistics for 14 matched $O_3$ VMR profiles from FTIR and smoothed MIPAS measurements at Addis Ababa. Means of the differences and standard deviations are shown.





AMTD
5, 6763–6812, 2012



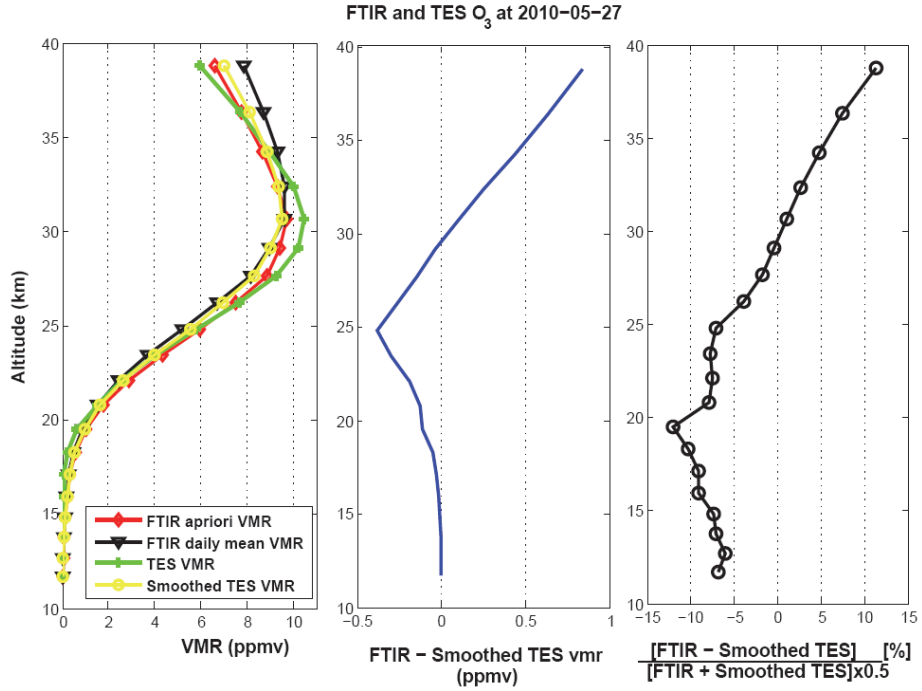


**Fig. 10.** Comparisons of $O_3$ VMR profiles from the FTIR and TES at Addis Ababa on 27 May 2010. On the left panel: $O_3$ VMR profiles of FTIR apriori (red with diamond symbol), FTIR daily mean (black with triangle symbol), TES smoothed (yellow with circle) and TES (green with plus sign symbol), as function of altitude. Differences between the FTIR and smoothed TES are shown with units of volume mixing ratio and % (solid line with circle) on the middle and right panels respectively.





AMTD
5, 6763–6812, 2012



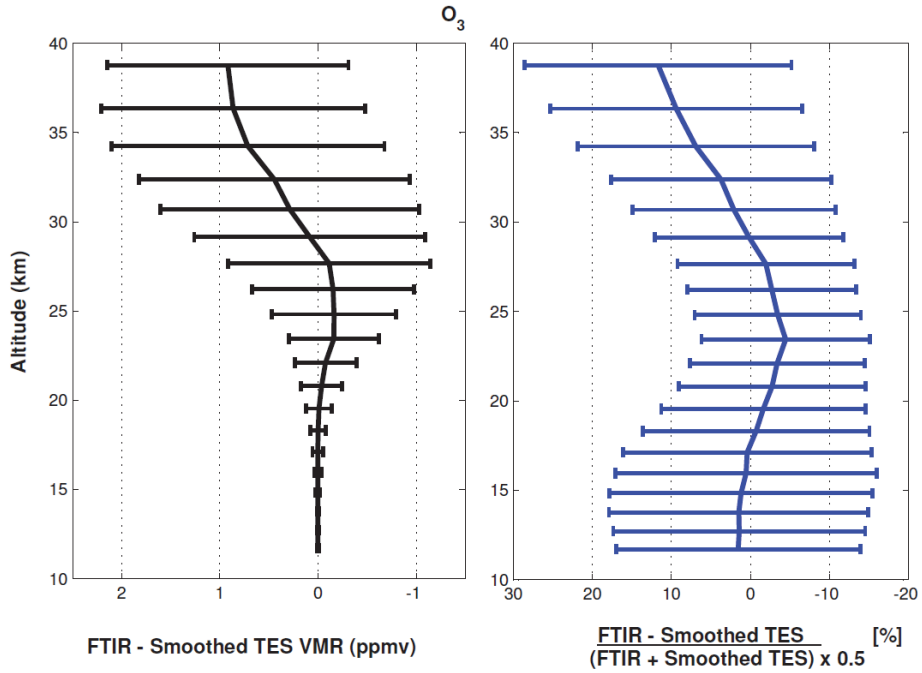


**Fig. 11.** Statistics for 13 matched $O_3$ VMR profiles from FTIR and smoothed TES measurements at Addis Ababa. Means of the differences and standard deviations are shown.





AMTD
5, 6763–6812, 2012



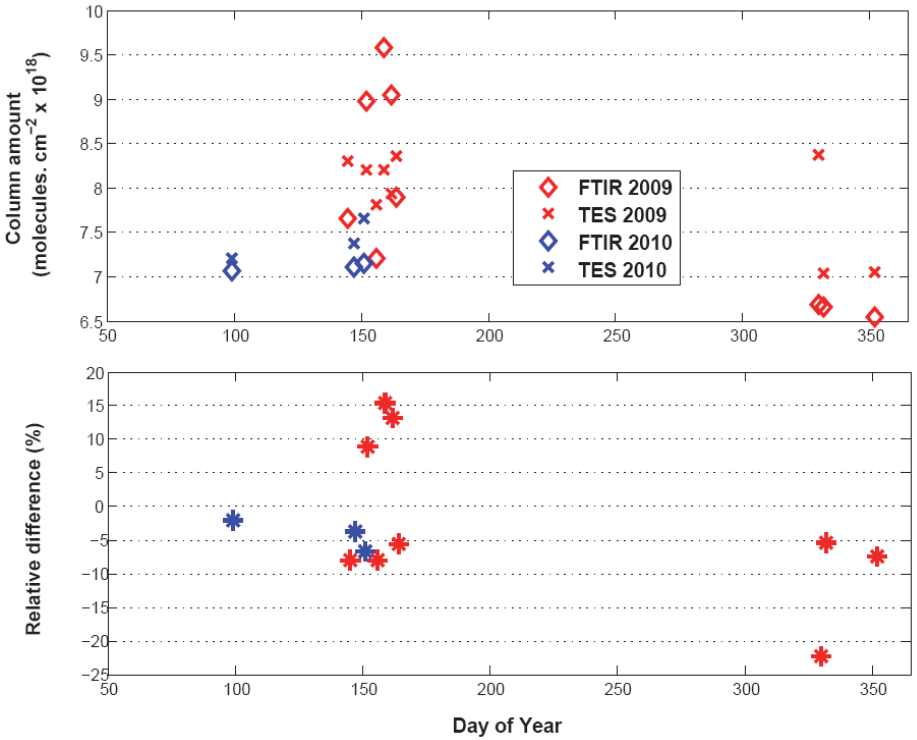


**Fig. 12.** The top panel shows the total column values $O_3$ for FTIR (open diamonds) and for the correlative TES measurements (cross). The bottom panel gives the relative differences between the column values of FTIR and TES (for 13 coincident measurements).





AMTD
5, 6763–6812, 2012



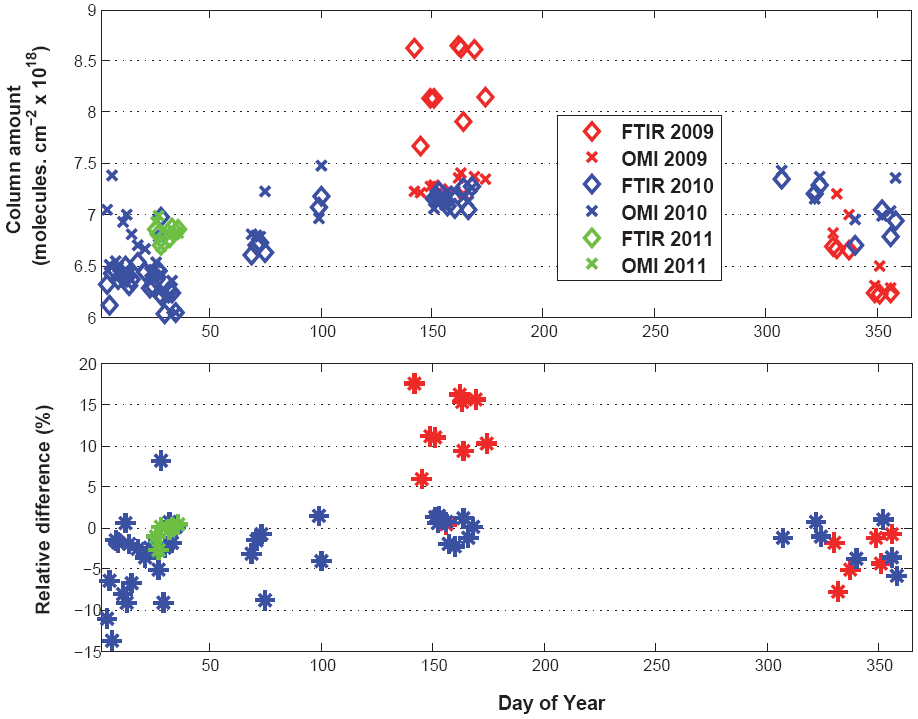


**Fig. 13.** The top panel shows the total column values $O_3$ for FTIR (open diamonds) and for the correlative OMI measurements (cross). The bottom panel gives the relative differences between the column values of FTIR and OMI (for 70 coincident measurements).





AMTD
5, 6763–6812, 2012



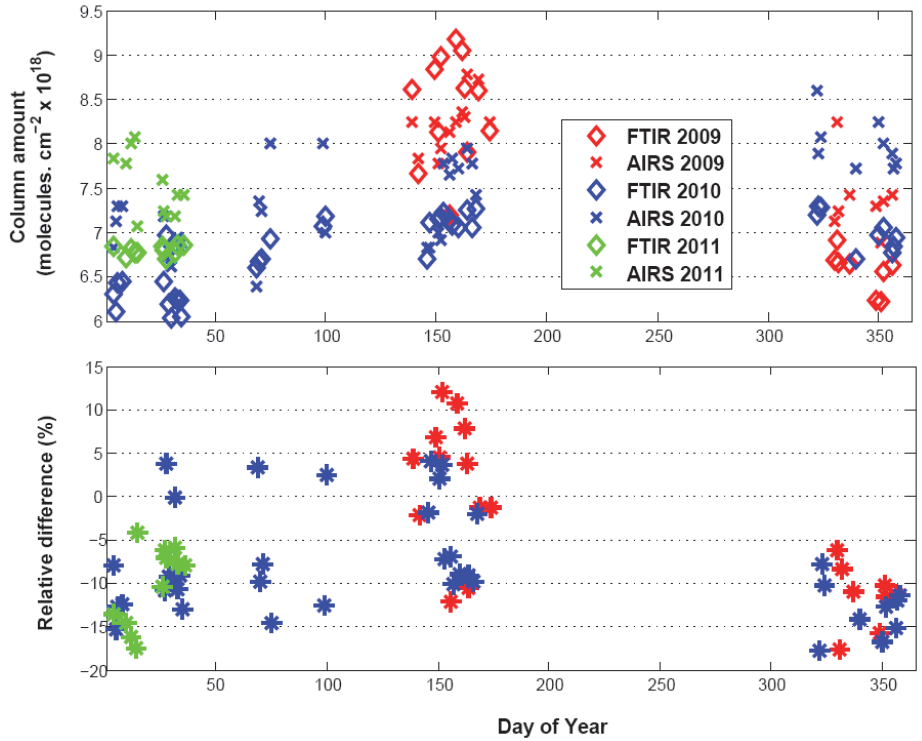


**Fig. 14.** The top panel shows the total column values $O_3$ for FTIR (open diamonds) and for the correlative AIRS measurements (cross). The bottom panel gives the relative differences between the column values of FTIR and AIRS (for 70 coincident measurements).





AMTD
5, 6763–6812, 2012



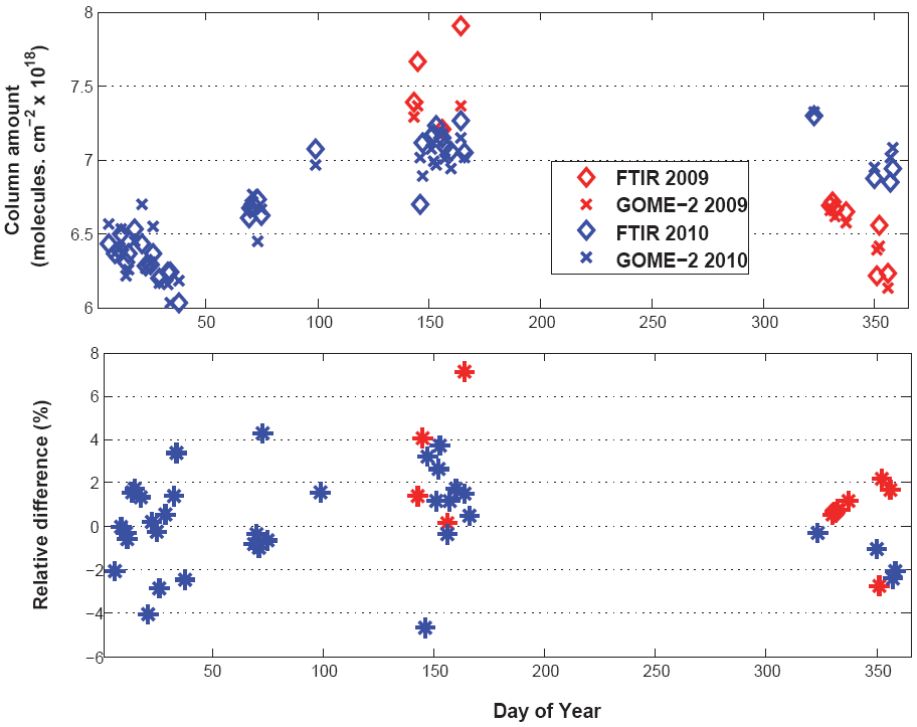


**Fig. 15.** The top panel shows the total column values $O_3$ for FTIR (open diamonds) and for the correlative GOME-2 measurements (cross). The bottom panel gives the relative differences between the column values of FTIR and GOME-2 (for 46 coincident measurements).





AMTD
5, 6763–6812, 2012



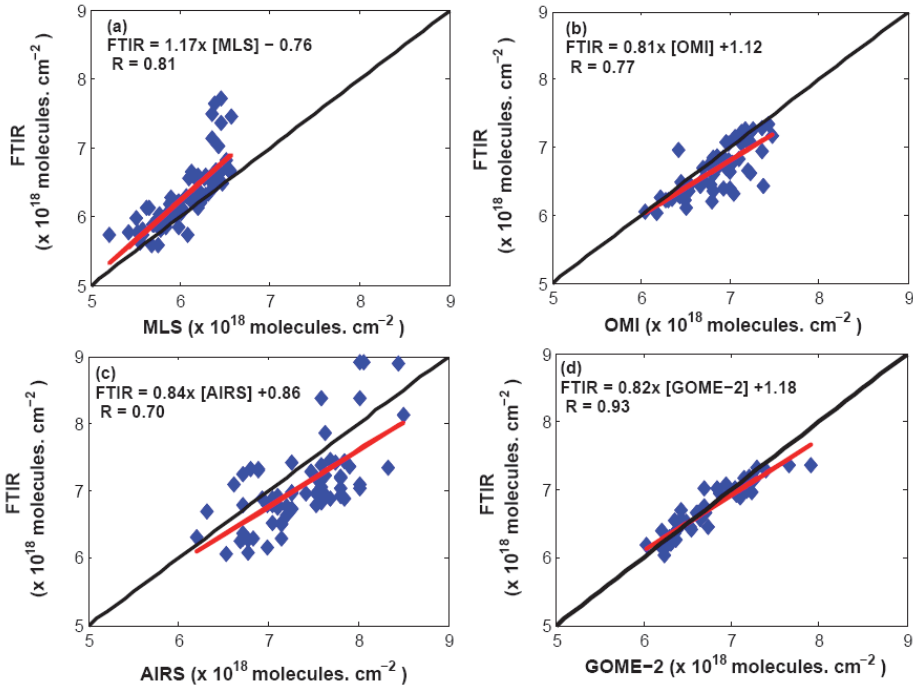


**Fig. 16.** Scatter plot of columns amount of $O_3$ measured by ground-based FTIR versus those observed by MLS, OMI, AIRS and GOME2. In all figures, the red line shows the fitted correlation function between the two data sets being compared. The slope and *R* for the comparisons are given on the plot. The black solid line shows the one-to-one relationship for the comparison.





AMTD
5, 6763–6812, 2012